Engineering new branches of the kynurenine pathway to produce oxo-(2-aminophenyl) and quinoline scaffolds in yeast

Michael Patrick Torrens-Spence[1†], Chun-Ting Liu[1,2,3†] and Jing-Ke Weng[1,2*]

[1]Whitehead Institute for Biomedical Research, 455 Main Street, Cambridge, MA 02142 USA.

[2]Department of Biology, Massachusetts Institute of Technology, Cambridge, MA 02139 USA.

[3]Department of Chemistry, Massachusetts Institute of Technology, Cambridge, MA 02139 USA.

[†]Co-first authors

*Corresponding author. Email: wengj@wi.mit.edu

GRAPHICAL ABSTRACT

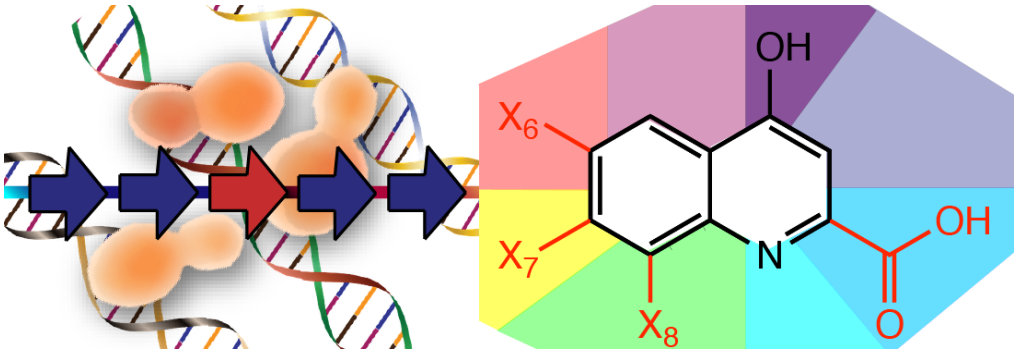

Keywords (4-6 words)

Kynurenine pathway

Kynurenine decarboxylase

Chlorokynurenine

Quinoline

ABSTRACT

The kynurenine pathway, named after its non-proteinogenic amino acid precursor L-kynurenine, is responsible for the *de novo* biosynthesis of nicotinamide adenine dinucleotide (NAD^+) in eukaryotes. Oxo-(2-aminophenyl) and quinoline molecules downstream from L-kynurenine also serve as antagonists of several receptors of the central nervous system in mammals. In this study, we engineered new biosynthetic routes in yeast *Saccharomyces cerevisiae* to produce a suite of L-kynurenine-derived natural products. Overexpression of *Homo sapiens* L-tryptophan 2,3-dioxygenase (*Hs*TDO2) in *S. cerevisiae* led to marked increase in the production of L-kynurenine and downstream metabolites. Using this background, new branch points to the kynurenine pathway were added through the incorporation of a *Psilocybe cubensis* noncanonical L-aromatic amino acid decarboxylase (*Pc*ncAAAD) capable of catalyzing both decarboxylation and decarboxylation-dependent oxidative-deamination reactions of L-kynurenine and 3-hydroxy-L-kynurenine to yield their corresponding monoamines, aldehydes, and downstream non-enzymatically cyclized quinolines. The *Pc*ncAAAD-catalyzed decarboxylation products, kynuramine and 3-hydroxykynuramine, could further be converted to quinoline scaffolds through the addition of *H. sapiens* monoamine oxidase A (*Hs*MAO-A). Finally, by incorporating upstream regiospecific L-tryptophan halogenases into the engineering scheme, we produced a number of halogenated oxo-(2-aminophenyl) and quinoline compounds. This work illustrates a synthetic-biology approach to expand primary metabolic pathways in the production of novel natural-product-like scaffolds amenable for downstream functionalization.

The planet Earth harbors an amazing diversity of life. Behind the apparent developmental and physiological differences between animals, plants, fungi, and microbes lies a hidden layer of chemical diversity, where diverging lineages have adopted unique evolutionary trajectories to arrive at new specialized metabolic traits [1]. In the biosynthetic logic of specialized metabolism, numerous families of scaffolding enzymes convert primary metabolic precursors into distinctive structural classes of natural products, whereas tailoring enzymes elaborate upon these scaffolds through reactions including but not limited to hydroxylation, prenylation, acylation, glycosylation, methylation, halogenation and sulfonation [1–3]. As many natural products with industrial and therapeutic utilities contain complex structures often difficult to be synthesized chemically, they are still routinely isolated from their native hosts. The deduction of native specialized metabolic pathways provides a biosynthetic basis for sustainable natural product production in heterologous hosts; however, *de novo* elucidation of unknown natural product biosynthetic pathways in nonmodel organisms remains challenging [4–8]. Although natural product semisynthesis can potentially bypass certain unknown biosynthetic steps, expensive intermediates, low yields, toxic byproducts, and difficulties in stereochemical synthesis often render the process commercially inviable [9–11]. Engineering natural product total biosynthesis in heterologous hosts with artificial pathways composed of enzymes selected for their biochemical activity rather than their native biosynthetic role therefore serves as an attractive alternative strategy [12].

Despite being greatly outnumbered by synthetic compounds, natural products and their derivatives are disproportionately overrepresented in human drugs [13–15]. The unique structural features possessed by natural products, key to their pharmacological

properties, are often missed in common scaffolds easily accessible through high-throughput organic synthesis [16]. As a result, exploration of biologically derived chemical scaffolds has the potential to yield alternative synthetic intermediates for existing or novel drugs [17]. In various medicinal plants, aromatic amino acids L-phenylalanine, L-tyrosine, and L-tryptophan give rise to a rich diversity of pharmacologically relevant phenylpropanoids, benzylisoquinoline alkaloids, and monoterpene indole alkaloids, respectively [18]. These native biosynthetic pathways have thus inspired metabolic engineering exercises to produce high-value phenolic and indolic compounds in alternative chassis organisms [18–20]. For example, previous studies have engineered metabolic pathways downstream of L-tyrosine in bacterial and fungal hosts to produce natural and new-to-nature opioids with therapeutic potential for treating pain [12,21–24]. The recent characterization of the *Psilocybe cubensis* psychotropic L-tryptophan-derived psilocybin pathway may likewise enable heterologous production of psilocybin analogs with therapeutic potential in the treatment of addiction, obsessive−compulsive disorders, and depression [25–28].

L-kynurenine, an L-tryptophan-derived non-proteinogenic amino acid, serves as the precursor for the kynurenine pathway required for the biosynthesis of nicotinamide adenine dinucleotide (NAD^+), and the neuroactive metabolites kynurenic acid (**2**) and xanthurenic acid (**3**) (**Figure 1**). Present in the brain and peripheral tissues, these quinoline carboxylic acids act upon several receptors of the human central nervous system (CNS), including the N-methyl-d-aspartate (NMDAR), α7 nicotinic acetylcholine (α7nAChR), and kainate receptors, to regulate neuronal physiology [29–32]. L-kynurenine and 3-hydroxy-L-kynurenine (**1**) are converted by kynurenine aminotransferase (KAT) to

their corresponding α-keto acids, which in turn cyclize through an intramolecular Schiff-base formation between the α-keto group and the oxo-(2-aminophenyl)-ring amine to yield the quinoline scaffold of **2** and **3**, respectively (**Figure S1**). Analogs of **2** and **3** were shown to display neuroprotective activities, suggesting that quinoline-derived molecules may find use in drug development for neurological diseases [33–36]. Moreover, the quinoline scaffold of **2** and **3** has served as an important lead scaffold for thousands of synthetic analogs and generations of the broad-spectrum antibiotics fluoroquinolones [37-38].

In this work, we engineer new metabolic branches from the kynurenine pathway using a substrate-promiscuous aromatic amino acid decarboxylase initially identified from *P. cubensis* (*Pc*ncAAAD) to produce oxo-(2-aminophenyl) and quinoline scaffolds in yeast *Saccharomyces cerevisiae*. Incorporation of several regio-specific L-tryptophan halogenases into the engineering scheme further yields additional halogenated analogs, including the candidate antidepressant prodrug 4-chlorokynurenine (**9**) and variants of the fluoroquinolone-class antibiotics [37,39]. The resulting metabolic engineering strategies enable access to new chemical entities that may find use in developing therapeutics for cognitive disorders, neurodegenerative impairment, and antimicrobials.

RESULTS

Branches from the kynurenine pathway can produce the quinoline scaffold

The kynurenine pathway is essential in eukaryotes for NAD^+ biogenesis. The NAD^+ biosynthetic pathway starts with the conversion of L-tryptophan to L-kynurenine, then oxidation of L-kynurenine to **1** which is further converted to NAD^+ (**Figure 1**) [40]. In an alternate pathway downstream of L-kynurenine, KAT catalyzes two-step transamination-

cyclization of L-kynurenine and **1** to produce **2** and **3**, respectively. Originally considered as an L-tryptophan catabolic process, this alternative pathway was recently shown to play roles in modulating immune system and neurological activities in mammals, where its dysregulation can lead to neuroinflammatory and neurodegenerative diseases [40,41]. The NMDA receptor antagonists **2** and **3** both contain quinoline scaffolds and are examples of heterocyclic natural products derived from nonenzymatic intramolecular Schiff-base formation. As both ketone and aldehyde can form Schiff base with a primary amine, the α-keto acids or aldehydes derived from L-kynurenine and **1** by the transaminase or aldehyde synthase activities respectively could cyclize to give two quinoline scaffolds differing by the presence/absence of the C2 carboxyl (**Figure S1**). We therefore reasoned that, by engineering non-native pathways branching from L-kynurenine or **1**, new heterocyclic-amine-derived molecules could be produced. First, to drive flux into L-kynurenine for further downstream pathway development and to minimize the metabolic shunt to NAD^+ production, we generated a yeast strain overexpressing *Homo sapiens tryptophan 2,3-dioxygenase* (*HsTDO2*). *Hs*TDO2 is a homotetramer heme-dependent enzyme capable of catalyzing the addition of molecular oxygen across the 2–3 bond of the indole moiety to convert L-tryptophan to N-formyl-L-kynurenine, which in turn decomposes *in vivo* to form L-kynurenine (**Figure 2a**) [42]. Overexpression of *HsTDO2* in yeast enhanced the formation of L-kynurenine and **1** by 25 and 47 fold, respectively (**Figure 2b**), while the accumulation of **2** and **3** from the downstream pathways were also increased (**Figure S2**). Interestingly, we also detected 4-hydroxyquinoline (**5**) and 4,8-dihydroxyquinoline (**7**) at very low levels in both wild-type and *Hs*TDO2-overexpressing yeast strains (**Figure S3**), which were likely derived from 3-(2-aminophenyl)-3-

oxopropanal and 3-(2-amino-3-hydroxyphenyl)-3-oxopropanal via the yeast Ehrlich pathway (**Figure S4**) [43]. To the best of our knowledge, this is the first time **5** and **7** are reported as yeast endogenous metabolites.

*Pc*ncAAAD contains both decarboxylase and aldehyde synthase activities toward L-kynurenine and 3-hydroxy-L-kynurenine substrates

Recent characterization of L-tryptophan decarboxylation chemistry in the hallucinogenic mushroom *P. cubensis* identified a noncanonical aromatic L-amino acid decarboxylases (*Pc*ncAAAD) with broad substrate promiscuity and a unique C-terminal appendage domain that confers calcium-dependent catalytic enhancement [44]. *Pc*ncAAAD catalyzes the decarboxylation of not only the proteinogenic aromatic amino acids L-phenylalanine, L-tyrosine, and L-tryptophan, but also the non-proteinogenic aromatic amino acids 5- and 7-chloro-L-tryptophan. Since the majority of previously characterized AAADs display a much narrower substrate preference, *Pc*ncAAAD provides a generally applicable tool for metabolic engineering of L-aromatic-amino-acid-derived natural products [23,45,46]. Given its substrate permissiveness, *Pc*ncAAAD may also accommodate L-kynurenine to produce the decarboxylated product kynuramine. This hypothesis is supported by molecular docking simulations showing that L-kynurenine and L-tryptophan adopt similar binding poses in the *Pc*ncAAAD active site (**Figure S5**). While kynuramine is presumably produced by L-3,4-dihydroxyphenylalanine (L-DOPA) decarboxylase (DDC) from L-kynurenine in mammalian cells [47], direct evidence supporting this notion is lacking.

Together with *Pc*ncAAAD, we screened several AAADs *in vitro* against L-kynurenine and 3-hydroxy-L-kynurenine (**1**), including *Catharanthus roseus* L-tryptophan

decarboxylase (*Cr*TDC), *Papaver somniferum* L-tyrosine decarboxylase (*Ps*TyDC), and *H. sapiens* L-DOPA decarboxylase (*Hs*DDC). *Cr*TDC and *Ps*TyDC are plant AAADs involved in the first step of different alkaloid biosynthetic pathways, with substrate preferences toward L-tryptophan and L-tyrosine, respectively [23,48]. *Hs*DDC is suggested to be responsible for trace monoamine formation, but principally catalyzes the decarboxylation of L-DOPA and 5-hydroxy-L-tryptophan to produce the mammal neurotransmitters dopamine and serotonin, respectively [49]. Amongst the screened AAADs, only *Pc*ncAAAD was able to utilize L-kynurenine and **1** as substrates (**Figure S6**). Intriguingly, the *in vitro* products of *Pc*ncAAAD include not only the decarboxylated monoamines **4** and **6** but also an additional product in each assay, which were subsequently confirmed to be 4-hydroxyquinoline (**5**) and 4,8-dihydroxyquinoline (**7**)**.** The formation of **5** and **7** is likely derived from aromatic acetaldehyde synthase (AAS) activity of *Pc*ncAAAD, i.e. decarboxylation-dependent oxidative deamination, followed by spontaneous cyclization (**Figure 2c**). Non-enzymatic oxidation to form these quinolinol scaffolds from their corresponding monoamines is unlikely as the **4** standard remained stable under identical reaction conditions. In addition, no aldehyde or cyclized product was observed when *Pc*ncAAAD was incubated with **4**, suggesting that the formation of **5** is directly from L-kynurenine.

Michaelis-Menten kinetic assays show that while *Pc*ncAAAD exhibits similar K_M values against L-kynurenine and L-tryptophan, the k_{cat} value for L-kynurenine is lower than that for L-tryptophan (**Table 1, Figure S7**). The calcium-activated increase in catalytic efficiency (k_{cat}/K_M) is also diminished from 546 fold for L-tryptophan to 21 fold for L-kynurenine, and indicates that L-kynurenine is unlikely to be the native substrate of

*Pc*ncAAAD. Overall, while *Pc*ncAAAD exhibits minimal aldehyde synthase activity toward preferential substrates such as L-tryptophan and L-tyrosine, it apparently contains significant aldehyde synthase activity toward non-native substrates L-kynurenine and **1**. When utilizing low-affinity substrates adopting nonoptimal binding configurations within the active site, oxygen likely enters the active site and acts as a co-substrate to facilitate the alternative decarboxylation-dependent oxidative deamination [23]. To the best of our knowledge, *Pc*ncAAAD is the first characterized AAAD capable of catalyzing both the decarboxylation and decarboxylation-oxidative-deamination reactions using nonnative amino acid substrates L-kynurenine and **1** to produce their corresponding monoamine and aromatic acetaldehyde products simultaneously. Overall, the dual activity and substrate permissiveness of *Pc*ncAAAD engenders a unique bioengineering tool for expanding the kynurenine pathway.

Coexpression of *Hs*TDO2, *Pc*ncAAAD, and *Hs*MAO-A leads to the production of decarboxylated hydroxyquinoline scaffolds in yeast

To examine the utility of *Pc*ncAAAD in expanding the kynurenine pathway *in vivo*, we introduced a *PcncAAAD*-containing plasmid into the *Hs*TDO2-overexpressing strain, and assessed the metabolic profile of the resultant transgenic yeast. Coexpression of both *Hs*TDO*2* and *Pc*ncAAAD in yeast resulted in a 106- and 184-fold increase in **5** and **7** levels, respectively, demonstrating the effectiveness of *Pc*ncAAAD in generating branching points from the kynurenine pathway *in vivo* (**Figure 2c-d**).

As only a fraction of the substrates L-kynurenine and **1** are converted to their desired heterocyclic products **5** and **7** by the *Pc*ncAAAD aldehyde synthase activity or

yeast endogenous enzymatic activities, we introduced an additional plasmid containing *H. sapiens monoamine oxidase A* (*HsMAO-A*) to enhance the conversion of **4** and **6** to **5** and **7**, respectively. *Hs*MAO-A has been extensively studied as this flavin-containing amine oxidoreductase is responsible for the mono-oxidation of dietary monoamines and neurotransmitters *in vivo* and is associated with numerous neurological disorders, including schizophrenia, depression, substance abuse, and attention deficit disorder [50,51]. The addition of *HsMAO-A* to the yeast strain coexpressing *HsTDO2* and *PcncAAAD* further drives flux toward the decarboxylated heterocyclic scaffolds as yields of **5** and **7** are enhanced (**Figure 3a-c**). It is likely that yeast FAD-utilizing polyamine oxidase (FMS1) additionally catalyzes this monoamine mono-oxidation reaction endogenously, as expression of *HsTDO2* and *PcncAAAD* in the *fms1* knockout strain displays the accumulation of monoamine **4** (**Figure S8**).

Next, we integrated *HsTDO2*, *PcncAAAD*, and *HsMAO-A* into a single plasmid under the control of constitutive *pTDH3* promoters, which we named pHQ for its ability to generate molecules with the hydroxyquinoline scaffold (**Figure 3d**). While the multi-gene vector increased the level of **5** and **7** by 417- and 2321-fold, respectively, as compared to wild type, the accumulation of these products remained low, with a measured **5** titer of 1.6 μg/L when grown aerobically in yeast nitrogen base (YNB) media using shake flasks. The levels of other branching metabolites including **2** and **3** were also similarly enhanced in pHQ-plasmid-containing yeast strains compared to wild type (**Figure S9**).

As *Pc*ncAAAD displays a calcium-dependent acceleration in activity *in vitro*, we additionally explored calcium supplementation *in vivo* for enhanced pHQ-derived product formation [44]. When the yeast growth medium YNB was supplemented with 0, 1, 5, or 10

mM calcium chloride, the production of **5** increased by a marginal 1.3-fold at 1 mM supplemented calcium but remained at similar or even lower levels when the supplemented calcium was above 5 mM, potentially due to toxicity of high concentrations of calcium (**Figure S10**). While the activation of *Pc*ncAAAD may be tunable *in vivo,* the background level of 0.9 mM calcium in YNB is probably approaching the saturation level for the *Pc*ncAAAD calcium-binding sites and precludes substantially more calcium-dependent catalytic acceleration.

The two-enzyme decarboxylation and oxidation pathway enables greater product formation than a single decarboxylation-dependent oxidative deamination enzyme

Naturally occurring AAAD and AAS paralogs in mammals, plants, insects, and fungi can be mechanistically interconverted through select active-site mutations [44,52–54]. As determined in the crystal structure of *Pc*ncAAAD, residue Y471 is likely the catalytic tyrosine that protonates the carbanion intermediate required for the decarboxylation chemistry [44,52]. In most AAADs, substitution of this catalytic tyrosine with phenylalanine or other bulky hydrophobic residues engenders AAS activity. Therefore, to explore aldehyde synthase chemistry in the single-enzyme conversion of L-kynurenine to **5**, we generated yeast expressing the catalytic mutant *Pc*ncAAAD^{Y471F}. Although coexpression of *Hs*TDO2 and *Pc*ncAAAD^{Y471F} led to the accumulation of **5** in yeast, the strain containing the pHQ multi-gene vector displayed a higher product titer (**Figure S11**). The lower **5** product formation in the *Hs*TDO2-*Pc*ncAAAD^{Y471F} strain could be attributable to a decrease in total catalytic efficiency of the *Pc*ncAAAD^{Y471F} mutant. Similar decreases in

substrate turnover have previously been observed in the interconversion of other AAAD-family enzymes [52].

Halogenated derivatives of quinoline compounds

Halogenated drugs often exhibit altered medicinal properties as compared to their un-substituted analogs. Consequently, halogenases are emerging as bioengineering tools to produce regio-selectively functionalized products from substrates of interest that would otherwise be hard to modify through synthetic chemistry [55]. Amongst the investigated halogenases, the flavin-dependent halogenases (FDHs) together with the flavin reductases required for FDH activity *in vivo* have been the best studied. The versatility of these enzymes in the halogenation of L-tryptophan, tryptophan-containing oligopeptides, and other larger indole-based substrates have been previously described [56–59]. The bacterial FDHs PyrH, ThdH, and RebH are well characterized enzymes that halogenate L-tryptophan at the 5, 6, and 7 position, respectively [60–62].

Coexpression of *PyrH*, *ThdH*, or *RebH* together with a corresponding flavin reductase gene *RebF* and pHQ resulted in the production of regio-specifically chlorinated analogs of L-kynurenine and **1**-**7** from the extend kynurenine pathway, namely chloro-L-kynurenine (**9**), chloro-3-hydroxy-L-kynurenine (**10**), chloro-2-carboxy-4-hydroxyquinoline (**11**), chloro-2-carboxy-4,8-dihydroxyquinoline (**12**), chlorokynuramine (**13**), chloro-4-hydroxyquinoline (**14**), and chloro-4,8-dihydroxyquinoline (**16**), which all show the characteristic isotope pattern of chlorinated compounds (**Figure 4** & **Figure S12**). We did not detect chloro-3-hydroxykynuramine (**15**); however, as **6** is known to be easily oxidized under physiological condition [63], the addition of a chlorine atom onto the

aromatic ring could have further destabilize the molecule. In addition, we did not observe 7-chloro-4-hydroxyquinoline (**14b**), 7-chloro-2-carboxy-4,8-dihydroxyquinoline (**12b**), and 7-chloro-4,8-dihydroxyquinoline (**16b**), indicating that *Hs*MAO-A may be less permissive of certain substituted aromatic substrates relative to the upstream *Hs*TDO2 or *Pc*ncAAAD enzymes.

As previous reports have demonstrated that FDHs can also use bromide to produce brominated L-tryptophan, we assessed the capacity of these enzymes to function in the bromination of kynurenine pathway metabolites *in vivo* [64]. When 50 mM sodium bromide was supplemented to the medium, brominated intermediates in the kynurenine pathway were observed, including bromo-kynurenine (**18**), bromo-3-hydroxy-L-kynurenine (**19**), bromo-2-carboxy-4-hydroxyquinoline (**20**), and bromo-4-hydroxyquinoline (**23**) (**Figure S13 & S14**). As no production of bromokynuramine (**22**), bromo-3-hydroxykynuramine (**24**), bromo-2-carboxy-4,8-dihydroxyquinoline (**21**), and bromo-4,8-dihydroxyquinoline (**25**) could be detected, the engineered pathway may be less permissive toward the structurally larger brominated substrates. Among these halogenated kynurenine-pathway products, 4-chloro-L-kynurenine (**9b**) and its structural analogs **9a** and **9c,** and the C2 carboxylic-acid-containing halogenated quinolones **11a**, **11b**, **11c** and **12a** are of particular interest as these compounds may potentially serve as neuropharmaceutical drug candidates and the basis of new fluoroquinolone antibiotics, respectively.

DISCUSSION

Devising synthetic biology strategies to gain access to valuable pharmaceuticals and commodity chemicals is key for the transition toward a sustainable and green chemical industry. In this work, we explore synthetic branches of the kynurenine pathway in *S. cerevisiae* to produce a number of functionalized oxo-(2-aminophenyl) and quinoline scaffolds. The quinoline derivatives have numerous applications ranging from metal complexes to nanoparticle development, and have also been extensively explored by medicinal chemists in the context of developing quinolone antibiotics. Since the discovery of nalidixic acid, over ten thousand analogs of the quinoline scaffold have been synthesized, from which generations of the broad-spectrum synthetic antibiotics have been developed [37,38]. These compounds and their subsequently halogenated fluoroquinolones represent the first class of fully synthetic antibacterial agents and are critical in treating both Gram-positive and Gram-negative bacterial infections. The molecular basis for the inhibition of bacterial type II topoisomerases, DNA gyrase, and DNA topoisomerase IV by the quinoline pharmacophores has been extensively studied over decades of research. As reported, the pharmacophore of fluoroquinolones comprises a bicyclic ring with eight chemical features underlying various structure–activity relationships [65]. In this work, through the expansion of the kynurenine pathway in yeast, we are able to vary the quinoline pharmacophore at the C2 ring position with a carboxyl group, the C6 or C7 ring positions with Cl or Br halogenation, and the C8 position with hydroxylation or halogenation. Importantly, while initial structure–activity relationship studies indicate that the carboxyl group at C2 interacts with the catalytic divalent metal ions of the target bacterial DNA gyrase and is crucial for inhibition, quinazolinediones lack

the C2 carboxyl, indicating that substitutions at this position may lead to new analogs for battling against quinolone antibiotic resistance [66].

In addition to the extensively explored quinoline scaffold, a growing body of evidence suggests that the precursory L-kynurenine and other oxo-(2-aminophenyl)-containing molecules in the kynurenine pathway may also find use in drug development. L-kynurenine itself is an inhibitor of α7nAChRs, an antagonist of NMDARs, and an activator of aryl hydrocarbon receptors (AHRs) [67–69]. The oxo-(2-aminophenyl)-containing **13a**, **13b**, and **13c** are of particular interest as these compounds function as neuropharmaceutical prodrug candidates [39]. Moreover, L-kynurenine and **9b** serve as biosynthetic precursors for the *Streptomyces sp.* cyclic lipopeptide antibiotics daptomycin and taromycin, respectively, where the oxo-(2-aminophenyl) moiety is essential for the antibiotic activity of the hexapeptide core [70,71]. Recently, bromo-L-kynurenine (**18**) and a number of downstream derivatives were also identified as the biofluorescent small molecules responsible for the blue-to-green fluorescence of certain sharks [72]. The fluorescent nature of halogenated L-kynurenine and downstream quinoline compounds [73] may be harnessed to devise future cell-based directed evolution experiments to enhance the production of L-kynurenine-derived molecules in heterologous hosts.

The rapid evolution of specialized metabolic systems gave rise to the remarkable chemical diversity in living organisms [74]. New enzyme activities emerge predominantly through gene duplication followed by sub- and neo-functionalization. In a previous study of the type II PLP decarboxylase enzymes in *P. cubensis*, we identified the substrate-promiscuous calcium-activatable *Pc*ncAAAD which may play a role in psilocybin biosynthesis [44]. A structural and mechanistic understanding of this noncanonical enzyme

has facilitated rational engineering of the desirable biochemical activities. As demonstrated here with the *Pc*ncAAAD^{Y471F} mutant, *Pc*ncAAAD activity can be toggled between decarboxylase and aldehyde synthase through mechanism-based mutagenesis [44,74]. In the expanded kynurenine pathway described in this work, the substrate permissiveness of *Pc*ncAAAD is required for L-kynurenine accommodation. However, this same broad substrate selectivity also results in an upstream metabolic shunt away from the L-kynurenine pathway, as *Pc*ncAAAD preferentially catalyzes the turnover of L-tryptophan over L-kynurenine. Future experiments may further refine substrate selectivities and/or catalytic properties of *Pc*ncAAAD for constructing specific routes of the L-kynurenine pathway.

In this work, we used L-tryptophan halogenases upstream of the kynurenine pathway to produce halogenated downstream oxo-(2-aminophenyl) and quinoline compounds. This strategy is similar to a previous report that generated halogenated vinca alkaloids through the use of L-tryptophan halogenases in *Catharanthus roseus* [75]. Nevertheless, the poor accommodation of halogenated intermediates by various downstream enzymes likely hindered final product yield. The recruitment of the chlorinated-substrate-specific TDO and kynurenine formamidase, identified from the *Saccharomonospora* sp. CNQ-490 taromycin A operon, could partially ameliorate this issue [76]. Alternatively, late-stage halogenases, as described in malbrancheamide biosynthesis, could potentially be adopted to functionalize the quinoline scaffold directly [75,77,78].

Collectively, this research opens a new avenue for the production of functionalized oxo-(2-aminophenyl) and quinoline scaffolds in yeast. Expansion of this engineered

metabolic pathway with alternative tailoring enzymes will provide further chemical diversity with potential industrial and medicinal utilities.

METHODS

Reagents

L-phenylalanine, phenylethylamine, L-tryptophan, tryptamine, L-DOPA, dopamine, L-kynurenine, 3-hydroxy-DL-kynurenine, kynuramine, and 4-quinolinol were purchased from Sigma-Aldrich and used as received.

Molecular Cloning

The coding sequences (CDS) of *PcncAAAD*, *HsTDO2*, and *HsDDC* were PCR amplified using *P. cubensis* or *H. sapiens* cDNA as template DNA with gene-specific primers (Supplemental Table 2). Internal BsaI and BsmBI restriction sites were abolished through Gibson-assembly-based mutagenesis using mutation oligonucleotides (Supplemental Table 2). The *HsMAO-A*, *RebH*, *RebF*, *ThdH* and *PyrH* genes were synthesized as gBlocks (IDT) with codon optimization specified for *S. cerevisiae*. The PCR amplicons or gBlocks were ligated into various base vectors via Gibson assembly or Golden Gate assembly. Destination vectors include the bacterial expression vector pHis8-4; the constitutive *S. cerevisiae* expression vectors p423TEF, p425TEF, and p426TEF [79] and a custom yeast toolkit multigene expression vector [79,80]. Transcriptional units and subsequent multigene vectors, assembled downstream of the yeast toolkit entry vector, were assembled through Golden Gate assembly for constitutive expression in *S. cerevisiae*.

Metabolomic profiling by liquid-chromatography high-resolution accurate-mass mass-spectrometry (LC-HRAM-MS)

Saturated starter cultures of S. cerevisiae, grown in 3 mL of yeast extract peptone dextrose (YPD) medium, were used to inoculate individual bioreactor conical tubes containing 15 mL of YNB minimal medium, dextrose, and the necessary auxotrophic markers. After 24 h of shaking at 30 °C, the cultures were pelleted by centrifugation, washed with water, and stored at −80 °C for subsequent metabolomic extraction. Frozen yeast pellets were disrupted using the Qiagen TissueLyser (Qiagen), zirconia beads, and 50% methanol (500 µL per 100 mg cell pellet weight). Lysates were clarified by centrifugation, filtered using 0.2 µm nano|filter vials (Thomson Instrument Company), and analyzed by LC-HRAM-MS following a previously described method 44. The raw data were converted to mzML format using MSConvert [81], and analyzed using MetaboAnalyst [82] and MZmine 2 [83].

Recombinant Protein Production and Purification

Escherichia coli BL21(DE3) cells containing various protein expression constructs were grown at 37 °C in terrific broth to OD600 of 0.9, induced with 0.15 mM isopropyl-β-D-thiogalactoside (IPTG), and grown for 20 h at 18 °C. The bacterial cells were harvested by centrifugation, washed with PBS (137 mM NaCl, 2.7 mM KCl, 10 mM Na_2HPO4, and 1.8 mM KH_2PO_4), resuspended in 150 mL of lysis buffer (50 mM Tris [pH 8.0], 0.5 M NaCl, 20 mM imidazole, 200 µM pyridoxal 5′-phosphate (PLP), and 0.5 mM dithiothreitol (DTT), and lysed with multiple passes through an M-110L microfluidizer (Microfluidics). The

resulting crude protein lysate was clarified by centrifugation prior to Qiagen nickel-nitrilotriacetic acid (Ni-NTA) gravity flow chromatographic purification. After passing the clarified lysate though the column, the resin was washed with 20-column volumes of lysis buffer and eluted with 1-column volume of elution buffer (50 mM Tris [pH 8.0], 0.5 M NaCl, 250 mM imidazole, 200 μM PLP, and 0.5 mM DTT). 1 mg of His-tagged tobacco etch virus (TEV) protease was added to the eluted protein, followed by dialysis at 4 °C for 16 h in dialysis buffer (50 mM Tris [pH 8.0], 0.1 M NaCl, 20 mM imidazole, 200 μM PLP, and 2 mM DTT). After dialysis, the protein solution was passed through Ni–NTA resin to remove the cleaved tag, the uncleaved recombinant protein, and His-tagged TEV. The flowthrough was further purified by gel filtration on a fast protein liquid chromatography (FPLC) system (GE Healthcare Life Sciences). The principal peaks were collected, buffer-exchanged using an Amicon Ultra-S15 centrifugal filter unit with Ultracel-30 membrane (EMD Millipore) and storage buffer (20 mM Tris [pH 8.0], 25 mM NaCl, 200 μM PLP, and 0.5 mM DTT), concentrated to a final protein concentration of 10 mg/mL, and flash frozen in liquid nitrogen. Prior to freezing, the *Pc*ncAAAD recombinant enzyme was further processed to remove metal ions though buffer exchange using a chelating buffer (50 mM imidazole, pH 8.0, 5 mM crown ether, 5 mM EDTA, 200 μM PLP, and 2 mM DTT) and then a metal-ion-free storage buffer (25 mM Tris, pH 7.5, 200 μM PLP, and 2 mM DTT). The purity of the recombinant proteins were evaluated by ImageJ2 densitometric analysis using BSA as the standard [84].

Enzyme Assays

The AAAD enzyme assays were performed in 100 µL of reaction buffer (50 mM Tris, pH 8.0) containing 2 µg of recombinant enzyme. Kinetic reactions were incubated with a range of L-kynurenine substrate concentrations (1 µM to 4 mM) at 25 °C for 30 min prior to quenching with 100 µL of 0.8 M formic acid. The reaction mixture was centrifuged and the supernatant was analyzed by liquid chromatography-mass spectrometry (LC-MS) coupled with a UV detector. 10 µL of reaction mixture was analyzed by an Ultimate 3000 liquid chromatography system (Dionex) equipped with a 150 mm C18 column (Kinetex 2.6 µm silica core shell C18 100 Å pore, Phenomenex), and coupled to an UltiMate 3000 diode-array detector in-line UV-Vis spectrophotometer (Dionex) and a TSQ Quantum Access MAX triple-quadrupole mass spectrometer (Thermo Fisher Scientific). Compounds were separated by reversed-phase chromatography with a ramp gradient of solvent A (0.1% formic acid in H_2O) and solvent B (0.1% formic acid in acetonitrile): 10% solvent B for 0.5 min, 5%–40% solvent B over 8.5 min, 95% solvent B for 1.8 min, followed by a final equilibration of 10% solvent B for 1 min with a flow rate at 0.7 mL/min. Product formation was measured using selected ion monitoring in positive mode for a centroid mass and a scan width of 0.5. Kynuramine product formation was quantified against a standard curve of kynuramine analytical standard. Kinetic constants such as k_{cat} and K_M were determined by fitting raw data to the Michaelis–Menten equation using the nonlinear regression function in Prism (version 7.0).

Molecular Docking

The docking simulations of L-kynurenine and L-tryptophan ligands into the active site of the *Pc*ncAAAD crystal structure (PDB accession 6EBN) [44] were conducted using

AutoDock Vina 1.1.2.42 [85]. The choice of grid and box size were determined as previously described [44].

AUTHOR INFORMATION

Supporting Information

The Supporting Information is available free of charge via the internet at http://pubs.acs.org.

Figure S1-S14 contain biosynthetic schemes of L-kynurenine-derived downstream products; quantification of various L-kynurenine pathway metabolites in transgenic yeast; Modeling of ligand binding in *Pc*ncAAAD structure; various AAAD *in vitro* enzyme activity and kinetic assays; and LC-MS chromatograms and isotope patterns of halogenated molecules produced from engineered yeast.

AUTHOR INFORMATION

Corresponding Author

*Email: wengj@wi.mit.edu

ORCID

Michael P. Torrens-Spence: 0000-0003-2644-1712

Chun-Ting Liu: 0000-0003-3996-5064

Jing-Ke Weng: 0000-0003-3059-0075

Author Contribution

M.P.T.S., C.T.L. and J.K.W. designed the research. M.P.T.S. and C.T.L. performed all experiments and analyzed and interpreted the data. M.P.T.S., C.T.L., and J.K.W. wrote the paper.

Funding

This work was supported by grants to Dr. Jing-Ke Weng from the Family Larsson-Rosenquist Foundation, the Pew Scholars Program in the Biomedical Sciences supported by the Pew Charitable Trusts, the Richard and Susan Smith Family Foundation, Newton, MA, the Searle Scholars Program, and the National Science Foundation (CHE-1709616).

Conflicts of Interest

J.K.W. is a co-founder, a member of the Scientific Advisory Board, and a shareholder of DoubleRainbow Biosciences, which develops biotechnologies related to natural products.

ACKNOWLEDGEMENTS

We thank Caroline Lewis, Bena Chan, and Tenzin Kunchok of the Whitehead Institute Metabolite Profiling Core Facility for assistance with the metabolomics data collection. Gerald Fink and Felix Lam kindly provided the yeast strains and yeast expression vectors used in this work. We thank Geoffrey Liou, Joseph Jacobowitz, Tomáš Pluskal, and Christopher Glinkerman for invaluable inputs to the writing this manuscript, and Tomáš Pluskal for support with the metabolomics analysis.

REFERENCES

(1) Weng, J.-K. The Evolutionary Paths towards Complexity: A Metabolic Perspective. *New Phytol.* **2014**, *201* (4), 1141–1149.
(2) Rey-Ladino, J.; Ross, A. G.; Cripps, A. W.; McManus, D. P.; Quinn, R. Natural Products and the Search for Novel Vaccine Adjuvants. *Vaccine* **2011**, *29* (38), 6464–6471.
(3) Anarat-Cappillino, G.; Sattely, E. S. The Chemical Logic of Plant Natural Product Biosynthesis. *Curr. Opin. Plant Biol.* **2014**, *19*, 51–58.
(4) Lau, W.; Sattely, E. S. Six Enzymes from Mayapple That Complete the Biosynthetic Pathway to the Etoposide Aglycone. *Science* **2015**, *349* (6253), 1224–1228.
(5) Torrens-Spence, M. P.; Pluskal, T.; Li, F.-S.; Carballo, V.; Weng, J.-K. Complete Pathway Elucidation and Heterologous Reconstitution of Rhodiola Salidroside Biosynthesis. *Mol. Plant* **2018**, *11* (1), 205–217.
(6) Pluskal, T.; Torrens-Spence, M. P.; Fallon, T. R.; De Abreu, A.; Shi, C. H.; Weng, J.-K. The Biosynthetic Origin of Psychoactive Kavalactones in Kava. *Nat. Plants* **2019**, 5, 867-878.
(7) Owen, C.; Patron, N. J.; Huang, A.; Osbourn, A. Harnessing Plant Metabolic Diversity. *Curr. Opin. Chem. Biol.* **2017**, *40*, 24–30.
(8) Tatsis, E. C.; O'Connor, S. E. New Developments in Engineering Plant Metabolic Pathways. *Curr. Opin. Biotechnol.* **2016**, *42*, 126–132.
(9) Paddon, C. J.; Westfall, P. J.; Pitera, D. J.; Benjamin, K.; Fisher, K.; McPhee, D.; Leavell, M. D.; Tai, A.; Main, A.; Eng, D.; et al. High-Level Semi-Synthetic Production of the Potent Antimalarial Artemisinin. *Nature* **2013**, *496* (7446), 528–532.
(10) Klein, J.; Heal, J. R.; Hamilton, W. D. O.; Boussemghoune, T.; Tange, T. Ø.; Delegrange, F.; Jaeschke, G.; Hatsch, A.; Heim, J. Yeast Synthetic Biology Platform Generates Novel Chemical Structures as Scaffolds for Drug Discovery. *ACS Synth. Biol.* **2014**, *3* (5), 314–323.
(11) Croteau, R.; Ketchum, R. E. B.; Long, R. M.; Kaspera, R.; Wildung, M. R. Taxol Biosynthesis and Molecular Genetics. *Phytochem. Rev*. 2006, pp 75–97.
(12) Galanie, S.; Thodey, K.; Trenchard, I. J.; Filsinger Interrante, M.; Smolke, C. D. Complete Biosynthesis of Opioids in Yeast. *Science* **2015**, *349* (6252), 1095–1100.
(13) Dias, D. A.; Urban, S.; Roessner, U. A Historical Overview of Natural Products in Drug Discovery. *Metabolites* **2012**, *2* (2), 303–336.
(14) Mishra, B. B.; Tiwari, V. K. Natural Products: An Evolving Role in Future Drug Discovery. *Eur. J. Med. Chem.* **2011**, *46* (10), 4769–4807.
(15) Li, F.-S.; Weng, J.-K. Demystifying Traditional Herbal Medicine with Modern Approach. *Nat. Plants* **2017**. 3, 17109.
(16) Ertl, P.; Roggo, S.; Schuffenhauer, A. Natural Product-Likeness Score and Its Application for Prioritization of Compound Libraries. *J. Chem. Inf. Model.* **2008**, *48* (1), 68–74.
(17) Ehrenworth, A. M.; Peralta-Yahya, P. Accelerating the Semisynthesis of Alkaloid-Based Drugs through Metabolic Engineering. *Nat. Chem. Biol.* **2017**, *13* (3), 249–258.
(18) Parthasarathy, A.; Cross, P. J.; Dobson, R. C. J.; Adams, L. E.; Savka, M. A.;

Hudson, A. O. A Three-Ring Circus: Metabolism of the Three Proteogenic Aromatic Amino Acids and Their Role in the Health of Plants and Animals. *Front. Mol. Biosci.* **2018**, *5*, 29.
(19) Gottardi, M.; Reifenrath, M.; Boles, E.; Tripp, J. Pathway Engineering for the Production of Heterologous Aromatic Chemicals and Their Derivatives in Saccharomyces Cerevisiae: Bioconversion from Glucose. *FEMS Yeast Res.* **2017**, *17 (4).*
(20) Bongaerts, J.; Krämer, M.; Müller, U.; Raeven, L.; Wubbolts, M. Metabolic Engineering for Microbial Production of Aromatic Amino Acids and Derived Compounds. *Metab. Eng.* **2001**, *3* (4), 289–300.
(21) DeLoache, W. C.; Russ, Z. N.; Narcross, L.; Gonzales, A. M.; Martin, V. J. J.; Dueber, J. E. An Enzyme-Coupled Biosensor Enables (S)-Reticuline Production in Yeast from Glucose. *Nat. Chem. Biol.* **2015**, *11* (7), 465–471.
(22) Nakagawa, A.; Matsuzaki, C.; Matsumura, E.; Koyanagi, T.; Katayama, T.; Yamamoto, K.; Sato, F.; Kumagai, H.; Minami, H. (R,S)-Tetrahydropapaveroline Production by Stepwise Fermentation Using Engineered Escherichia Coli. *Sci. Rep.* **2014**. 4, 6695.
(23) Torrens-Spence, M. P.; Chiang, Y.-C.; Smith, T.; Vicent, M. A.; Wang, Y.; Weng, J.-K. Structural Basis for Independent Origins of New Catalytic Machineries in Plant AAAD Proteins. *BioRxiv*. https://doi.org/10.1101/404970.
(24) Vavricka, C. J.; Yoshida, T.; Kuriya, Y.; Takahashi, S.; Ogawa, T.; Ono, F.; Agari, K.; Kiyota, H.; Li, J.; Ishii, J.; et al. Mechanism-Based Tuning of Insect 3,4-Dihydroxyphenylacetaldehyde Synthase for Synthetic Bioproduction of Benzylisoquinoline Alkaloids. *Nat. Commun.* **2019**, *10* (1), 2015.
(25) Johnson, M. W.; Garcia-Romeu, A.; Cosimano, M. P.; Griffiths, R. R. Pilot Study of the 5-HT2AR Agonist Psilocybin in the Treatment of Tobacco Addiction. *J. Psychopharmacol.* **2014**, *28* (11), 983–992.
(26) Fricke, J.; Blei, F.; Hoffmeister, D. Enzymatic Synthesis of Psilocybin. *Angew. Chem. Int. Ed Engl.* **2017**, *56* (40), 12352–12355.
(27) Moreno, F. A.; Wiegand, C. B.; Taitano, E. K.; Delgado, P. L. Safety, Tolerability, and Efficacy of Psilocybin in 9 Patients with Obsessive-Compulsive Disorder. *J. Clin. Psychiatry* **2006**, *67* (11), 1735–1740.
(28) Carhart-Harris, R. L.; Bolstridge, M.; Day, C. M. J.; Rucker, J.; Watts, R.; Erritzoe, D. E.; Kaelen, M.; Giribaldi, B.; Bloomfield, M.; Pilling, S.; et al. Psilocybin with Psychological Support for Treatment-Resistant Depression: Six-Month Follow-Up. *Psychopharmacology* **2018**, *235* (2), 399–408.
(29) Ruddick, J. P.; Evans, A. K.; Nutt, D. J.; Lightman, S. L.; Rook, G. A. W.; Lowry, C. A. Tryptophan Metabolism in the Central Nervous System: Medical Implications. *Expert Rev. Mol. Med.* **2006**, *8* (20), 1–27.
(30) Anderson, G.; Maes, M. Interactions of Tryptophan and Its Catabolites With Melatonin and the Alpha 7 Nicotinic Receptor in Central Nervous System and Psychiatric Disorders: Role of the Aryl Hydrocarbon Receptor and Direct Mitochondria Regulation. *Int. J. Tryptophan Res.* **2017**, *10*, 1178646917691738.
(31) Majláth, Z.; Török, N.; Toldi, J.; Vécsei, L. Memantine and Kynurenic Acid: Current Neuropharmacological Aspects. *Curr. Neuropharmacol.* **2016**, *14* (2), 200–209.

(32) Hilmas, C.; Pereira, E. F. R.; Alkondon, M.; Rassoulpour, A.; Schwarcz, R.; Albuquerque, E. X. The Brain Metabolite Kynurenic Acid Inhibits α7 Nicotinic Receptor Activity and Increases Non-α7 Nicotinic Receptor Expression: Physiopathological Implications. *J. Neurosci*. **2001**, *21* (19) 7463–7473.
(33) Acuña-Castroviejo, D.; Tapias, V.; López, L. C.; Doerrier, C.; Camacho, E.; Carrión, M. D.; Mora, F.; Espinosa, A.; Escames, G. Protective Effects of Synthetic Kynurenines on 1-Methyl-4-Phenyl-1,2,3,6-Tetrahydropyridine-Induced Parkinsonism in Mice. *Brain Res. Bull.* **2011**, *85* (3-4), 133–140.
(34) Wu, H. Q.; Lee, S. C.; Schwarcz, R. Systemic Administration of 4-Chlorokynurenine Prevents Quinolinate Neurotoxicity in the Rat Hippocampus. *Eur. J. Pharmacol.* **2000**, *390* (3), 267–274.
(35) Gellért, L.; Fuzik, J.; Göblös, A.; Sárközi, K.; Marosi, M.; Kis, Z.; Farkas, T.; Szatmári, I.; Fülöp, F.; Vécsei, L.; et al. Neuroprotection with a New Kynurenic Acid Analog in the Four-Vessel Occlusion Model of Ischemia. *Eur. J. Pharmacol*. **2011**, *667* (1-3), 182–187.
(36) Marosi, M.; Nagy, D.; Farkas, T.; Kis, Z.; Rózsa, E.; Robotka, H.; Fülöp, F.; Vécsei, L.; Toldi, J. A Novel Kynurenic Acid Analogue: A Comparison with Kynurenic Acid. An in Vitro Electrophysiological Study. *J. Neural Transm.* **2010**, *117* (2), 183–188.
(37) Lesher, G. Y.; Froelich, E. J.; Gruett, M. D.; Bailey, J. H.; Brundage, R. P. 1,8-NAPHTHYRIDINE DERIVATIVES. A NEW CLASS OF CHEMOTHERAPEUTIC AGENTS. *J. Med. Pharm. Chem.* **1962**, *91*, 1063–1065.
(38) Emmerson, A. M. The Quinolones: Decades of Development and Use. *J. Antimicrob. Chemother*. **2003**, *51* (suppl 1), 13–20.
(39) Zanos, P.; Piantadosi, S. C.; -Q. Wu, H.; Pribut, H. J.; Dell, M. J.; Can, A.; Snodgrass, H. R.; Zarate, C. A.; Schwarcz, R.; Gould, T. D. The Prodrug 4-Chlorokynurenine Causes Ketamine-Like Antidepressant Effects, but Not Side Effects, by NMDA/GlycineB-Site Inhibition. *J. Pharmacol. Exp. Ther*. **2015**, *35* (7), 76–85.
(40) Davis, I.; Liu, A. What Is the Tryptophan Kynurenine Pathway and Why Is It Important to Neurotherapeutics? *Expert Rev. Neurother*. **2015**, *15* (7), 719–721.
(41) Lovelace, M. D.; Varney, B.; Sundaram, G.; Franco, N. F.; Ng, M. L.; Pai, S.; Lim, C. K.; Guillemin, G. J.; Brew, B. J. Current Evidence for a Role of the Kynurenine Pathway of Tryptophan Metabolism in Multiple Sclerosis. *Front. Immunol.* **2016**, *7*, 246.
(42) Yan, D.; Lin, Y.-W.; Tan, X. Heme-Containing Enzymes and Inhibitors for Tryptophan Metabolism. *Metallomics* **2017**, *9* (9), 1230–1240.
(43) Hazelwood, L. A.; Daran, J.-M.; van Maris, A. J. A.; Pronk, J. T.; Dickinson, J. R. The Ehrlich Pathway for Fusel Alcohol Production: A Century of Research on Saccharomyces Cerevisiae Metabolism. *Appl. Environ. Microbiol.* **2008**, *74* (8), 2259–2266.
(44) Torrens-Spence, M. P.; Liu, C.-T.; Pluskal, T.; Chung, Y. K.; Weng, J.-K. Monoamine Biosynthesis via a Noncanonical Calcium-Activatable Aromatic Amino Acid Decarboxylase in Psilocybin Mushroom. *ACS Chem. Biol.* **2018**, *13* (12), 3343–3353.
(45) Han, Q.; Ding, H.; Robinson, H.; Christensen, B. M.; Li, J. Crystal Structure and

Substrate Specificity of Drosophila 3,4-Dihydroxyphenylalanine Decarboxylase. *PLoS One* **2010**, *5* (1), e8826.
(46) Bertoldi, M.; Borri Voltattorni, C. Reaction and Substrate Specificity of Recombinant Pig Kidney Dopa Decarboxylase under Aerobic and Anaerobic Conditions. *Biochim. Biophys. Acta* **2003**, *1647* (1-2), 42–47.
(47) Kaseda, H.; Noguchi, T.; Kido, R. Biosynthetic Routes to 2-Aminoacetophenone and 2-Amino-3-Hydroxyacetophenone. *J. Biochem.* **1973**, *74* (1), 127–133.
(48) Torrens-Spence, M. P.; Lazear, M.; von Guggenberg, R.; Ding, H.; Li, J. Investigation of a Substrate-Specifying Residue within Papaver Somniferum and Catharanthus Roseus Aromatic Amino Acid Decarboxylases. *Phytochemistry* **2014**, 106, 37–43.
(49) Burkhard, P.; Dominici, P.; Borri-Voltattorni, C.; Jansonius, J. N.; Malashkevich, V. N. Structural Insight into Parkinson's Disease Treatment from Drug-Inhibited DOPA Decarboxylase. *Nat. Struct. Biol.* **2001**, *8* (11), 963–967.
(50) Cashman, J. R. Monoamine Oxidases and Flavin-Containing Monooxygenases. *Compr. Toxicol*. **2018**, 10, 87–125.
(51) Singer, T. P. Monoamine Oxidases. In *Chemistry and Biochemistry of Flavoenzymes (II)*. Muller, F., Ed.; CRC Press: London **1991**, pp 437–470.
(52) Torrens-Spence, M. P.; Liu, P.; Ding, H.; Harich, K.; Gillaspy, G.; Li, J. Biochemical Evaluation of the Decarboxylation and Decarboxylation-Deamination Activities of Plant Aromatic Amino Acid Decarboxylases. *J. Biol. Chem.* **2013**, *288* (4), 2376–2387.
(53) Bertoldi, M.; Gonsalvi, M.; Contestabile, R.; Voltattorni, C. B. Mutation of Tyrosine 332 to Phenylalanine Converts Dopa Decarboxylase into a Decarboxylation-Dependent Oxidative Deaminase. *J. Biol. Chem.* **2002**, *277* (39), 36357–36362.
(54) Liang, J.; Han, Q.; Ding, H.; Li, J. Biochemical Identification of Residues That Discriminate between 3,4-Dihydroxyphenylalanine Decarboxylase and 3,4-Dihydroxyphenylacetaldehyde Synthase-Mediated Reactions. *Insect Biochem. Mol. Biol.* **2017**, *91*, 34–43.
(55) Walker, M. C.; Thuronyi, B. W.; Charkoudian, L. K.; Lowry, B.; Khosla, C.; Chang, M. C. Y. Expanding the Fluorine Chemistry of Living Systems Using Engineered Polyketide Synthase Pathways. *Science* **2013**, *341* (6150), 1089–1094.
(56) Heemstra, J. R., Jr; Walsh, C. T. Tandem Action of the O2- and FADH2-Dependent Halogenases KtzQ and KtzR Produce 6,7-Dichlorotryptophan for Kutzneride Assembly. *J. Am. Chem. Soc.* **2008**, *130* (43), 14024–14025.
(57) Smith, D. R. M.; Uria, A. R.; Helfrich, E. J. N.; Milbredt, D.; van Pée, K.-H.; Piel, J.; Goss, R. J. M. An Unusual Flavin-Dependent Halogenase from the Metagenome of the Marine Sponge Theonella Swinhoei WA. *ACS Chem. Biol.* **2017**, *12* (5), 1281–1287.
(58) Ortega, M. A.; Cogan, D. P.; Mukherjee, S.; Garg, N.; Li, B.; Thibodeaux, G. N.; Maffioli, S. I.; Donadio, S.; Sosio, M.; Escano, J.; et al. Two Flavoenzymes Catalyze the Post-Translational Generation of 5-Chlorotryptophan and 2-Aminovinyl-Cysteine during NAI-107 Biosynthesis. *ACS Chem. Biol.* **2017**, *12* (2), 548–557.
(59) Neubauer, P. R.; Widmann, C.; Wibberg, D.; Schröder, L.; Frese, M.; Kottke, T.;

Kalinowski, J.; Niemann, H. H.; Sewald, N. A Flavin-Dependent Halogenase from Metagenomic Analysis Prefers Bromination over Chlorination. *PLoS One* **2018**, *13* (5), e0196797.
(60) Zehner, S.; Kotzsch, A.; Bister, B.; Süssmuth, R. D.; Méndez, C.; Salas, J. A.; van Pée, K.-H. A Regioselective Tryptophan 5-Halogenase Is Involved in Pyrroindomycin Biosynthesis in Streptomyces Rugosporus LL-42D005. *Chem. Biol.* **2005**, *12* (4), 445–452.
(61) Seibold, C.; Schnerr, H.; Rumpf, J.; Kunzendorf, A.; Hatscher, C.; Wage, T.; Ernyei, A. J.; Dong, C.; Naismith, J. H.; Van Pée, K.-H. A Flavin-Dependent Tryptophan 6-Halogenase and Its Use in Modification of Pyrrolnitrin Biosynthesis. *Biocatal. Biotransform*. **2006**, *24* (6), 401–408.
(62) Sánchez, C.; Butovich, I. A.; Braña, A. F.; Rohr, J.; Méndez, C.; Salas, J. A. The Biosynthetic Gene Cluster for the Antitumor Rebeccamycin: Characterization and Generation of Indolocarbazole Derivatives. *Chem. Biol.* **2002**, *9* (4), 519–531.
(63) Li, J.; Beerntsen B. T.; James A. A. Oxidation of 3-Hydroxykynurenine to Produce Xanthommatin for Eye Pigmentation: A Major Branch Pathway of Tryptophan Catabolism during Pupal Development in the Yellow Fever Mosquito, Aedes Aegypti. *Insect Biochem. Mol. Biol*. **1999**, *29* (4), 329–338.
(64) van Pée, K. H. Microbial Biosynthesis of Halometabolites. *Arch. Microbiol.* **2001**, *175* (4), 250–258.
(65) Singh, S.; Kaur, G.; Mangla, V.; Gupta, M. K. Quinoline and Quinolones: Promising Scaffolds for Future Antimycobacterial Agents. *J. Enzyme Inhib. Med. Chem.* **2015**, *30* (3), 492–504.
(66) Aldred, K. J.; Kerns, R. J.; Osheroff, N. Mechanism of Quinolone Action and Resistance. *Biochemistry*. **2014**, *53* (10), 1565–1574.
(67) Albuquerque, E. X.; Schwarcz, R. Kynurenic Acid as an Antagonist of α7 Nicotinic Acetylcholine Receptors in the Brain: Facts and Challenges. *Biochem Pharmacol*. **2013**, *85* (8), 1027–1032.
(68) Stone, T. W. Endogenous Neurotoxins from Tryptophan. *Toxicon* **2001**, *39* (1), 61–73.
(69) Nguyen, N. T.; Nakahama, T.; Le, D. H.; Van Son, L.; Chu, H. H.; Kishimoto, T. Aryl Hydrocarbon Receptor and Kynurenine: Recent Advances in Autoimmune Disease Research. *Front. Immunol.* **2014**, *5*, 551.
(70) Liao, G.; Wang, L.; Liu, Q.; Guan, F.; Huang, Y.; Hu, C. Manipulation of Kynurenine Pathway for Enhanced Daptomycin Production in Streptomyces Roseosporus. *Biotechnol. Prog.* **2013**, *29* (4), 847–852.
(71) Reynolds, K. A.; Luhavaya, H.; Li, J.; Dahesh, S.; Nizet, V.; Yamanaka, K.; Moore, B. S. Isolation and Structure Elucidation of Lipopeptide Antibiotic Taromycin B from the Activated Taromycin Biosynthetic Gene Cluster. *J. Antibiot.* **2018**, *71* (2), 333–338.
(72) Park, H. B.; Lam, Y. C.; Gaffney, J. P.; Weaver, J. C.; Krivoshik, S. R.; Hamchand, R.; Pieribone, V.; Gruber, D. F.; Crawford, J. M. Bright Green Biofluorescence in Sharks Derives from Bromo-Kynurenine Metabolism. *iScience* **2019**. 19:1291-1336.
(73) Jun, J. V.; Petersson, E. J.; Chenoweth, D. M. Rational Design and Facile Synthesis of a Highly Tunable Quinoline-Based Fluorescent Small-Molecule

Scaffold for Live Cell Imaging. *J. Am. Chem. Soc.* **2018**, *140* (30), 9486–9493.
(74) Weng, J.-K.; Philippe, R. N.; Noel, J. P. The Rise of Chemodiversity in Plants. *Science* **2012**, *336* (6089), 1667–1670.
(75) Runguphan, W.; Qu, X.; O'Connor, S. E. Integrating Carbon–halogen Bond Formation into Medicinal Plant Metabolism. *Nature* **2010**, *468* (7322), 461–464.
(76) Yamanaka, K.; Reynolds, K. A.; Kersten, R. D.; Ryan, K. S.; Gonzalez, D. J.; Nizet, V.; Dorrestein, P. C.; Moore, B. S. Direct Cloning and Refactoring of a Silent Lipopeptide Biosynthetic Gene Cluster Yields the Antibiotic Taromycin A. *Proc. Natl. Acad. Sci. U. S. A.* **2014**, *111* (5), 1957–1962.
(77) Martínez-Luis, S.; Rodríguez, R.; Acevedo, L.; González, M. C.; Lira-Rocha, A.; Mata, R. Malbrancheamide, a New Calmodulin Inhibitor from the Fungus Malbranchea Aurantiaca. *Tetrahedron*. **2006**, *62* (8), 1817–1822.
(78) Fraley, A. E.; Sherman, D. H. Halogenase Engineering and Its Utility in Medicinal Chemistry. *Bioorg. Med. Chem. Lett.* **2018**, *28* (11), 1992–1999.
(79) Mumberg, D.; Müller, R.; Funk, M. Yeast Vectors for the Controlled Expression of Heterologous Proteins in Different Genetic Backgrounds. *Gene* **1995**, *156* (1), 119–122.
(80) Lee, M. E.; DeLoache, W. C.; Cervantes, B.; Dueber, J. E. A Highly Characterized Yeast Toolkit for Modular, Multipart Assembly. *ACS Synth. Biol.* **2015**, *4* (9), 975–986.
(81) Chambers, M. C.; Maclean, B.; Burke, R.; Amodei, D.; Ruderman, D. L.; Neumann, S.; Gatto, L.; Fischer, B.; Pratt, B.; Egertson, J.; et al. A Cross-Platform Toolkit for Mass Spectrometry and Proteomics. *Nat. Biotechnol.* **2012**, *30* (10), 918–920.
(82) Xia, J.; Wishart, D. S. Using MetaboAnalyst 3.0 for Comprehensive Metabolomics Data Analysis. *Curr. Protoc. Bioinf.* **2016**, *55*, 14.10.1–14.10.91.
(83) Pluskal, T.; Castillo, S.; Villar-Briones, A.; Oresic, M. MZmine 2: Modular Framework for Processing, Visualizing, and Analyzing Mass Spectrometry-Based Molecular Profile Data. *BMC Bioinf.* **2010**, *11*, 395.
(84) Rueden, C. T.; Schindelin, J.; Hiner, M. C.; DeZonia, B. E.; Walter, A. E.; Arena, E. T.; Eliceiri, K. W. ImageJ2: ImageJ for the next Generation of Scientific Image Data. *BMC Bioinf.* **2017**, *18* (1), 529.
(85) Trott, O.; Olson, A. J. AutoDock Vina: Improving the Speed and Accuracy of Docking with a New Scoring Function, Efficient Optimization, and Multithreading. *J. Comput. Chem.* **2010**, *31* (2), 455–461.

Table

Table 1. Kinetics parameters of *Pc*ncAAAD toward L-kynurenine, L-phenylalanine, and L-tryptophan. Reactions were performed in 50 mM Tris, pH 8.0, and 30 mM sodium chloride or calcium acetate reaction buffer at 25 °C. Note that previous characterization of *Pc*ncAAAD demonstrated that this enzyme also readily catalyzes the decarboxylation L-tyrosine, although the turnover rate and Michaelis-Menten kenetic constants were ultimately not determined as the maximum rate of the reaction was limited by the solubility of the substrate [44].

Substrates		**30 mM Na^+**	**30 mM Ca^{2+}**
L-kynurenine	k_{cat} (sec^{-1})	0.19 ± 0.02	3.75 ± 0.12
	K_M (mM)	0.40 ± 0.14	0.38 ± 0.05
	k_{cat}/K_M (sec^{-1} mM^{-1})	0.47	9.75
L-phenylalanine*	k_{cat} (sec^{-1})	9.68 ± 0.28	3044.00 ± 263.80
	K_M (mM)	0.82 ± 0.07	0.78 ± 0.21
	k_{cat}/K_M (sec^{-1} mM^{-1})	11.80	3902.56
L-tryptophan*	k_{cat} (sec^{-1})	0.60 ± 0.06	255.40 ± 16.23
	K_M (mM)	0.45 ± 0.16	0.36 ± 0.09
	k_{cat}/K_M (sec^{-1} mM^{-1})	1.33	709.44

*kinetics results from previous study [44]

Figures

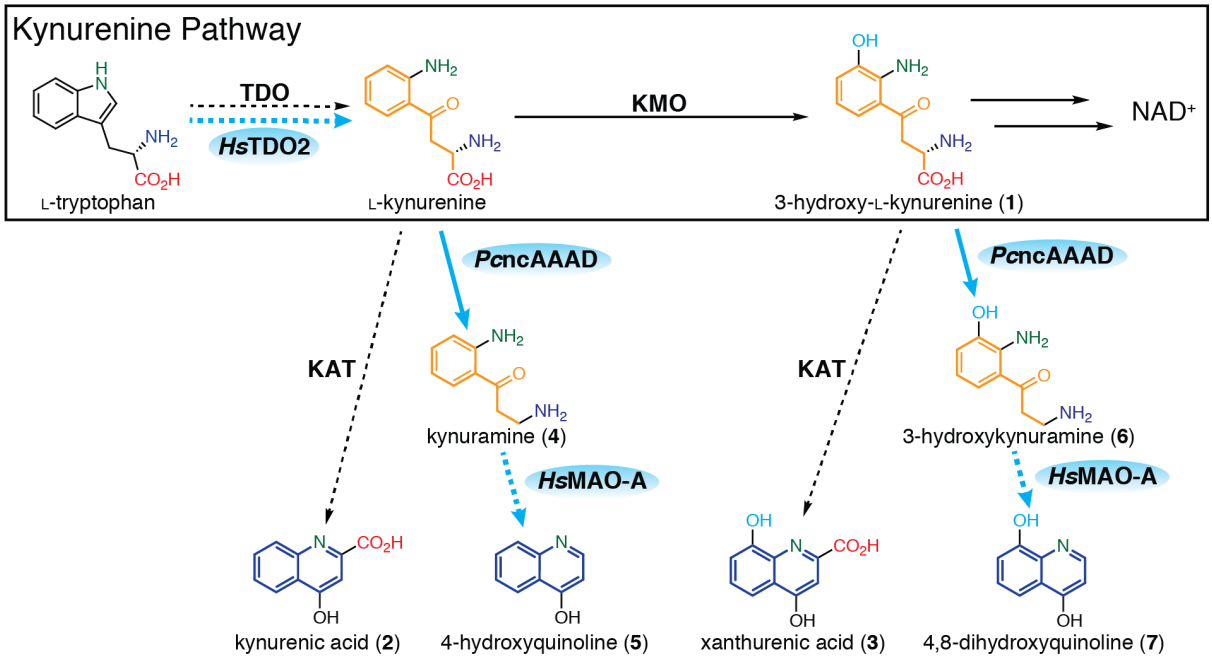

Figure 1 | Overview of the endogenous and engineered kynurenine pathways in yeast in this study. The endogenous kynurenine pathway in yeast requires TDO, KMO, and other enzymes for the *de novo* NAD^+ biosynthesis from L-tryptophan. KAT creates two branches from the kynurenine pathways that produce **2** and **3**, from L-kynurenine and **1**, respectively. By introducing *Hs*TDO2, *Pc*ncAAAD, and *Hs*MAO-A in yeast, we are able to increase the flux through the kynurenine pathway and add new pathways for the heterologous production of quinoline-core molecules with potential industrial interest. Note that *Pc*ncAAAD is also capable of producing **5** and **7** directly from L-kynurenine and **1** through its latent aldehyde synthase activity. The oxo-(2-aminophenyl) scaffold is highlighted in orange, and quinoline scaffold is highlighted in blue. Engineered pathways in this study are indicated by blue arrows, while previously known enzymatic steps in yeast are represented by black arrows. Dotted lines denote enzymatic steps with unstable intermediates not shown. Heterologous enzymes expressed in yeast are highlighted by blue ovals. TDO, tryptophan 2,3-dioxygenase; KMO, kynurenine 3-monooxygenase; KAT, kynurenine aminotransferase; *Hs*TDO2, *Homo sapiens* tryptophan 2,3-dioxygenase; *Pc*ncAAAD, *Psilocybe cubensis* non-canonical aromatic amino acid decarboxylase; *Hs*MAO-A, *H. sapiens* monoamine oxidase.

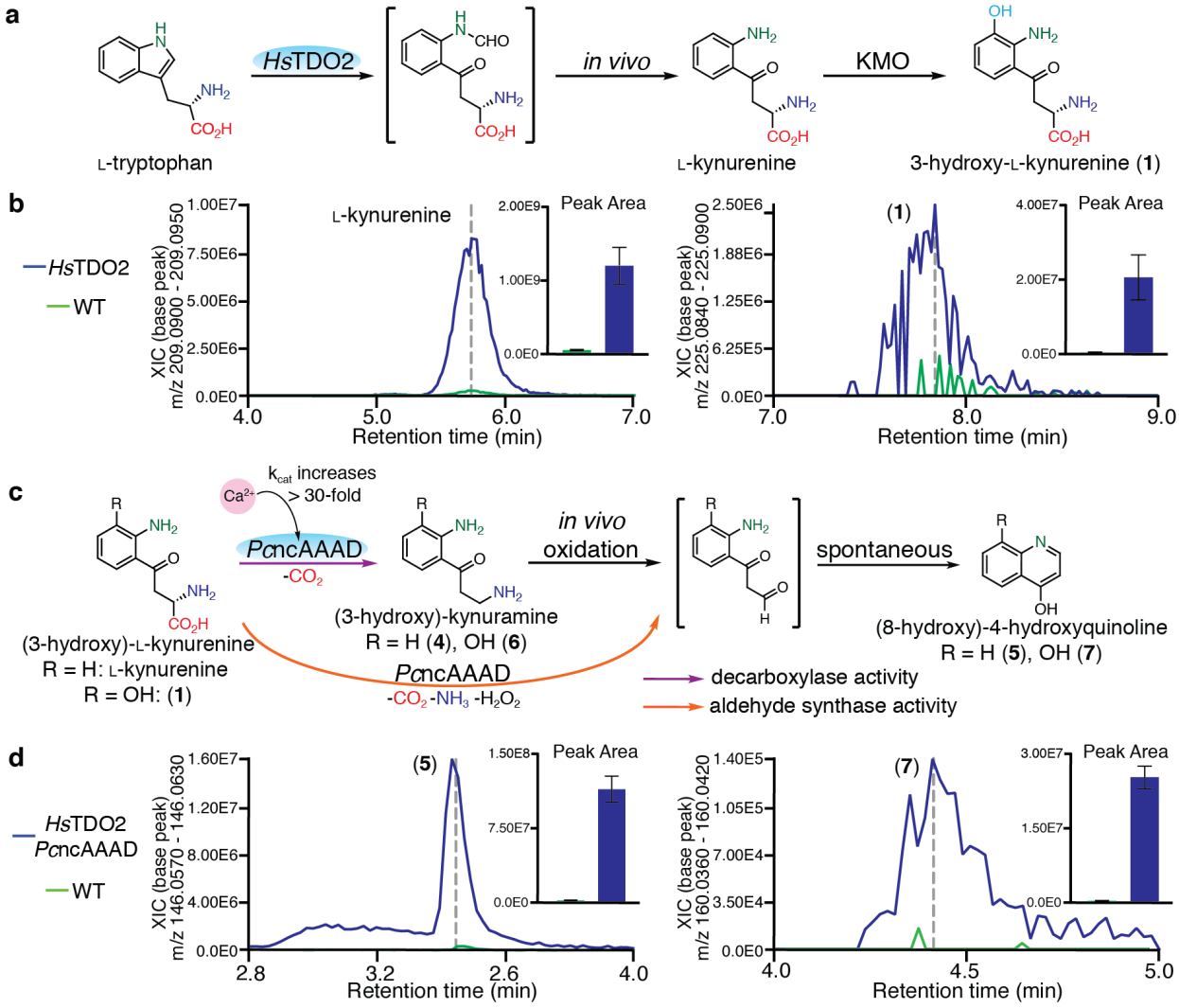

Figure 2 | Characterization of the biochemical activities of *Hs*TDO2 and *Pc*ncAAAD in the context of engineering new kynurenine pathway branches in yeast. (**a**) *Hs*TDO2 catalyzes the ring-opening of L-tryptophan to N-formyl-L-kynurenine, which is rapidly degraded to L-kynurenine *in vivo* and further converted to 3-hydroxy-L-kynurenine (**1**) by KMO. Heterologous enzymes expressed in yeast are highlighted by blue ovals. (**b**) Compared to wild type (WT) yeast, *Hs*TDO2-overexpressing yeast over-accumulates L-kynurenine and **1** by 25- and 47-fold, respectively. Bar graphs indicate the integrated peak area of the corresponding compounds. (**c**) The *in vivo* formation of **5** and **7** is derived from the aromatic acetaldehyde synthase (AAS) activity of *Pc*ncAAAD, which performs decarboxylation-dependent oxidative deamination to yield aromatic acetaldehyde products that spontaneously cyclize to **5** and **7**. The *in vitro* formation of **5** and **7** in *Hs*TDO2-

*Pc*ncAAAD-overexpressing yeast can be derived from both decarboxylase and AAS activities. In addition, *Pc*ncAAAD exhibits a calcium-activatable decarboxylation activity toward both L-kynurenine and **1**. (**d**) Compared to WT yeast, *Hs*TDO2-*Pc*ncAAAD-overexpressing yeast over-accumulates **5** and **7** by 106- and 184-fold, respectively. Error bars represent standard error of the mean (SEM) of biological triplicates.

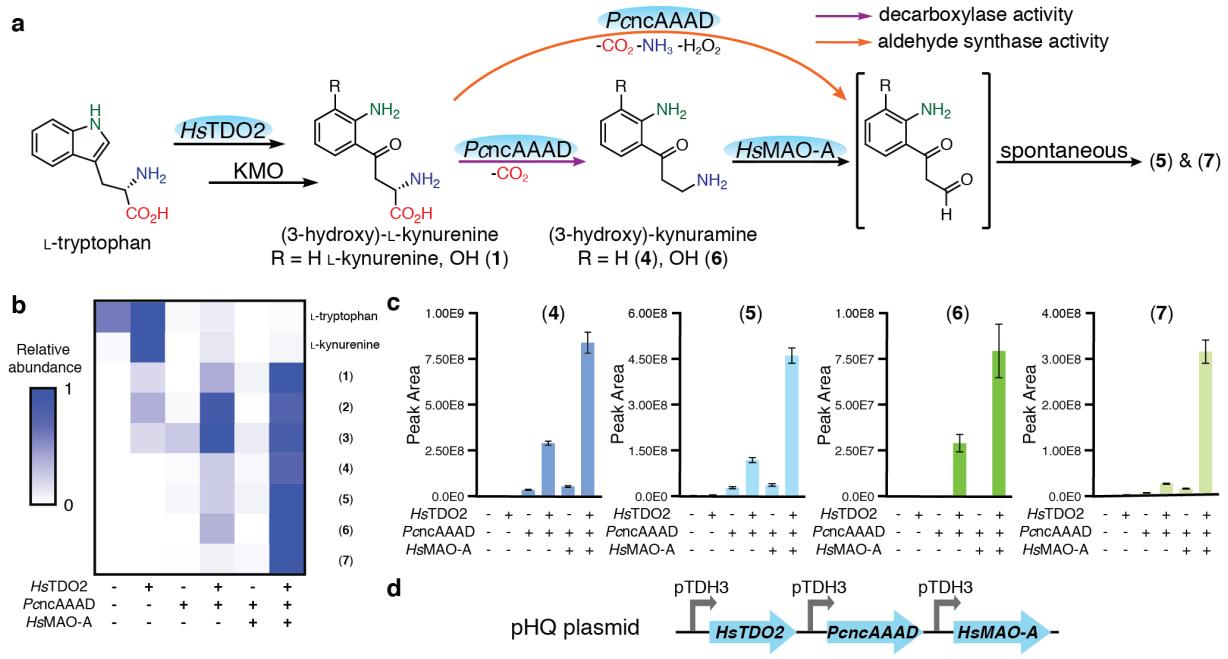

Figure 3 | Engineered metabolic pathway incorporating *Hs*TDO2, *Pc*ncAAAD, and *Hs*MAO-A to produce quinoline molecules in yeast. (**a**) The reaction scheme of the engineered kynurenine branch pathway from L-tryptophan to **5** and **7**. Heterologous enzymes expressed in yeast are highlighted by blue ovals. In this pathway, only the KMO enzyme is endogenous in yeast. (**b**) Relative abundance of select metabolites in several engineered yeast strains, where *Hs*TDO2, *Pc*ncAAAD, and *Hs*MAO-A are expressed either alone or in combination. Averaged integrated peak area of each compound based on biological triplicates is displayed. (**c**) Relative abundance of quinoline-core molecules **4**, **5**, **6**, and **7** in various engineered yeast strains. Error bars represent SEM of biological triplicates. (**d**) *HsTDO2*, *PcncAAAD*, and *HsMAO-A* are constructed into a single plasmid, which we termed pHQ, for its ability to produce hydroxyquinoline (HQ)-derived molecules.

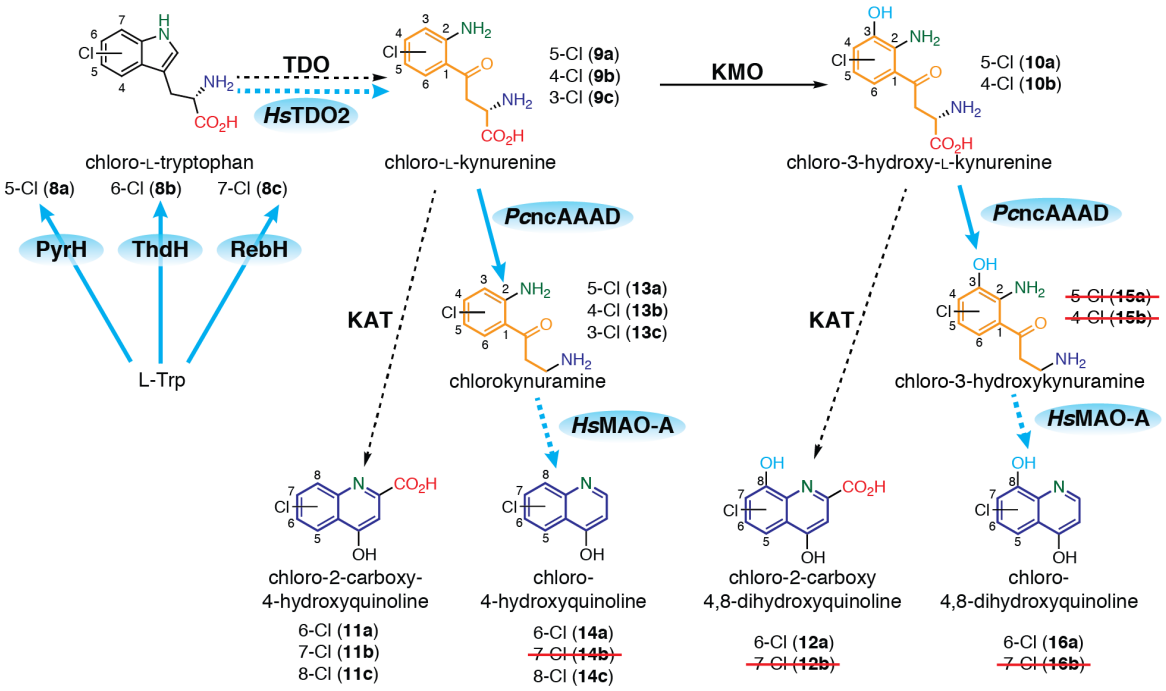

Figure 4 | Engineered metabolic pathway to produce chlorinated kynurenine-pathway molecules. The regio-specific halogenases PyrH, ThdH, or RebH produce the halogenated L-tryptophan substrate for the expanded kynurenine pathway in the production of the chlorinated intermediates **8**-**16**. Similar to the expanded kynurenine pathway shown in **Figure 1**, compounds **8**-**16**, which are analogs of L-kynurenine and **1**-**7** with chlorination at different positions on the aromatic ring, were produced in engineered yeast. The LC-MS traces and isotope patterns of these molecules are shown in **Figure S11**. Compound names crossed with a red line were not detected in engineered yeast, which could be due to either the instability of the molecules or the inability of *Hs*MAO-A to accommodate 4-chlorinated kynuramine substrates. RebH, tryptophan 7-halogenase; ThdH, tryptophan 6-halogenase; PyrH, tryptophan 5-halogenase.

Supporting Information for

Engineering new branches of the kynurenine pathway to produce oxo-(2-aminophenyl) and quinoline scaffolds in yeast

Michael Patrick Torrens-Spence[1†], Chun-Ting Liu[1,2,3†] and Jing-Ke Weng[1,2*]

[1]Whitehead Institute for Biomedical Research, 455 Main Street, Cambridge, MA 02142 USA.

[2]Department of Biology, Massachusetts Institute of Technology, Cambridge, MA 02139 USA.

[3]Department of Chemistry, Massachusetts Institute of Technology, Cambridge, MA 02139 USA.

[†]Co-first authors

*Corresponding author. Email: wengj@wi.mit.edu

Supplementary Figures

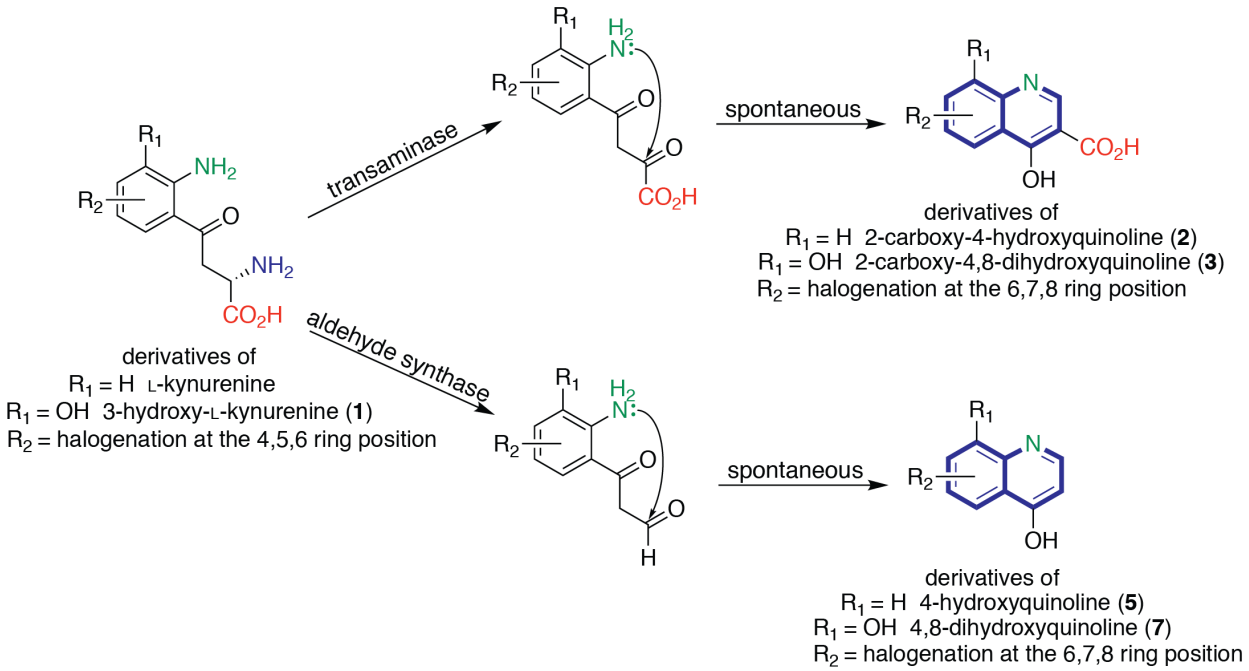

Figure S1 | L-Kynurenine and 1 derivatives can form molecules with quinoline scaffolds. L-kynurenine or **1** can undergo kynurenine aminotransferase (KAT)-mediated or aldehyde synthase-mediated pathways to form quinoline-core molecules. The immediate ketone or aldehyde products of the KAT or aldehyde synthase enzymes spontaneously cyclize to yield various quinoline derivatives. Quinoline scaffold is colored in blue.

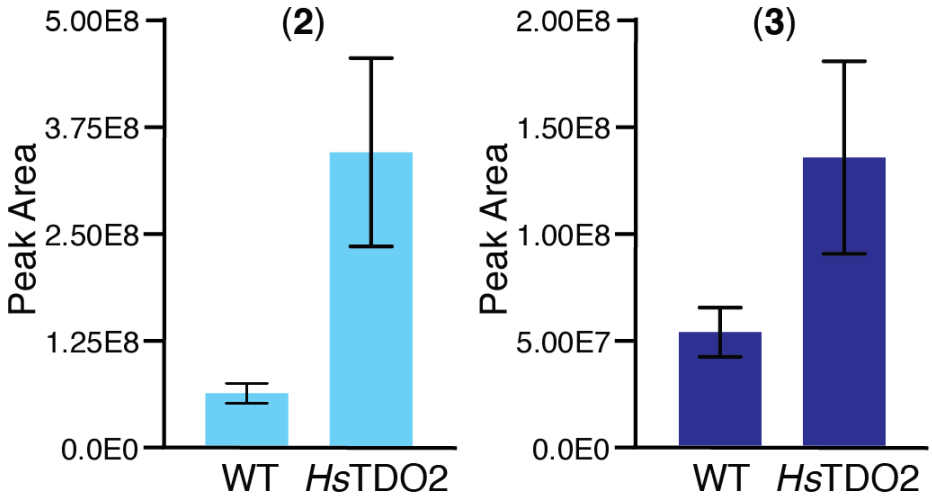

Figure S2 | Increased production of kynurenine pathway branching products 2 and 3 in *HsTDO2*-overexpressed yeast strain. The bar graphs represent the integrated peak areas of the corresponding compounds. Compared to wild-type (WT) yeast strain, the production of **2** and **3** increased by 6- and 2.5-fold, respectively. Error bars represent standard error of the mean (SEM) of biological triplicates.

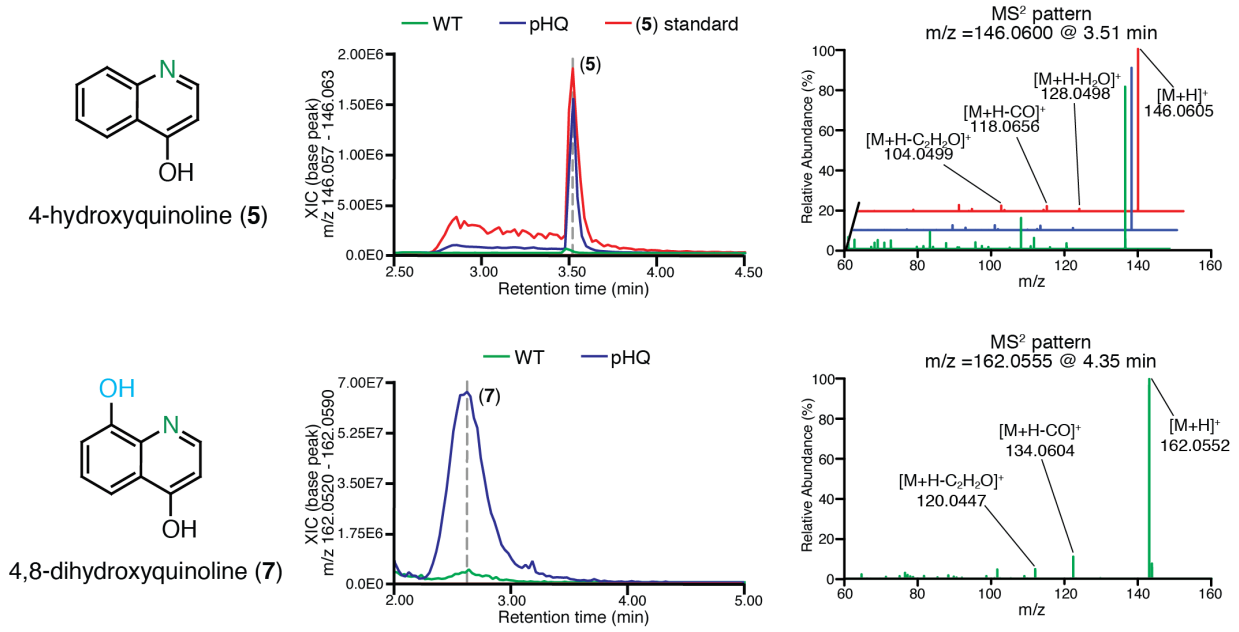

Figure S3 | Production of 5 and 7 in WT yeast. Compound **5** and **7** were detected in WT yeast despite the absence of exogenous L-kynurenine or 3-hydroxy-L-kynurenine decarboxylase. (**a**) The chromatogram (top panel) and MS/MS spectra at m/z = $[M+H]^+$ (bottom panel) of **5** standard confirm the presence of **5** in WT yeast. (**b**) While **7** standard was not available, **5** and **7** share a similar MS/MS fragmentation pattern given their structural similarity, which helped us to indirectly confirm the identity of **7**.

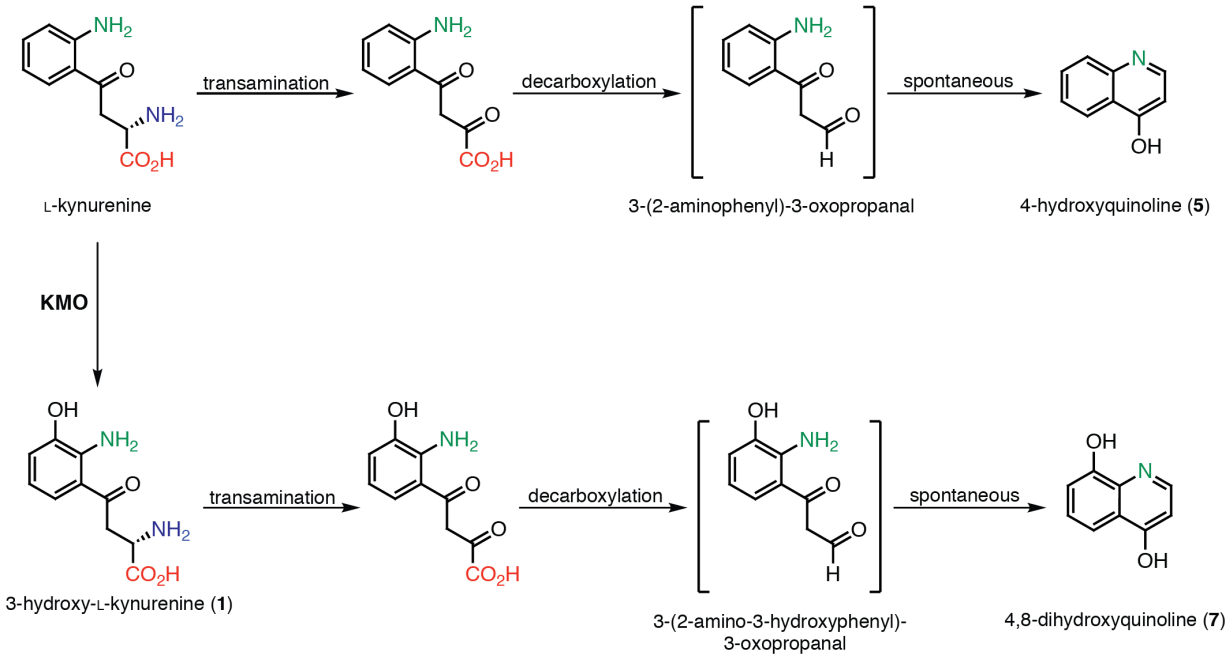

Figure S4 | Proposed Ehrlich pathway in yeast for the biosynthesis of 5 and 7. The Ehrlich pathway in yeast consists of two steps: transamination and decarboxylation of amino acids, which generates the corresponding α-keto acids and "fusel aldehydes". The fusel aldehydes are usually further oxidized or reduced into "fusel acid" or "fusel alcohol". In our proposed pathway, non-proteinogenic amino acids L-kynurenine and **1** undergo transamination and decarboxylation to yield their corresponding aldehydes, which spontaneously cyclize into **5** and **7**. Note that the Ehrlich pathway is essentially our engineered pathway in a reverse reaction order, with decarboxylation and transamination/oxidation being the two reactions involved. In addition, it is possible that the phenylpyruvate decarboxylase of the Ehrlich pathway could directly decarboxylate kynuramine-derived **2** and **3** to produce **5** and **7**, respectively. KMO, kynurenine 3-monooxygenase.

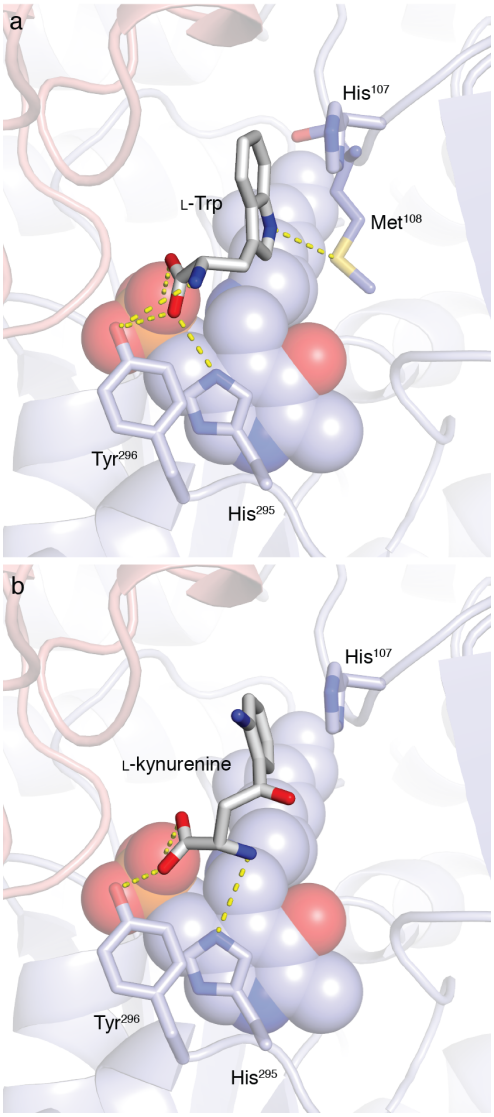

Figure S5 | Modeled binding orientations of L-tryptophan (a) and L-kynurenine (b) in the *Pc*ncAAAD active site. L-Tryptophan and L-kynurenine have similar modeled orientations in the *Pc*ncAAAD active site, with their aromatic rings forming pi-pi interactions with His^{107} and their amino and carboxyl groups interact with His^{295}, Tyr^{296}, and the phosphate group of the covalently bound lysine-pyridoxal-5'-phosphate (LLP) through hydrogen bonds. The binding calculated affinities are -6.1 and -6.2 kcal/mol for L-tryptophan- and L-kynurenine-docked models, respectively. The LLP is displayed as spheres, whereas residues putatively contributing to the binding of substrates are shown as sticks. *Pc*ncAAAD monomer A and B are shown in salmon and light blue, respectively. Simulated docking was performed using AutoDock Vina 1.1.2.

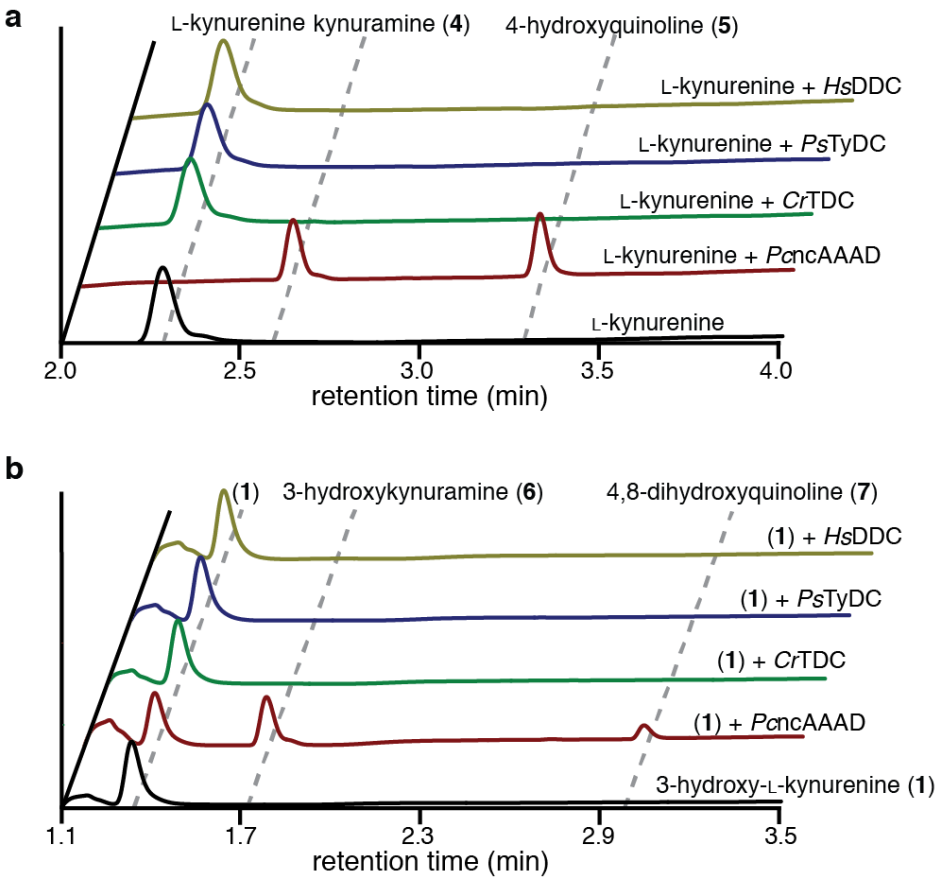

Figure S6 | AAADs activity assays toward L-kynurenine (a) and 3-hydroxy-L-kynurenine (1) (b). *Pc*ncAAAD, *Cr*TDC, *Ps*TyDC, and *Hs*DDC were screened for their activity toward L-kynurenine and **1**. Only *Pc*ncAAAD utilized L-kynurenine and **1** as substrates to produce kynuramine **4** and **6**. We were unable to measure any enzymatic activity of the recombinant *Hs*DDC against L-kynurenine or its native substrate L-DOPA, suggesting a possible problem with the *in vitro* assay condition or the activity of the purified *Hs*DDC enzyme. *Pc*ncAAAD also produced **5** and **7**, which are likely resulted from the spontaneously cyclized aldehyde products due to the aldehyde synthase activity. The assay was conducted in 50 mM Tris (pH 8.0) with 30 mM sodium chloride and reacted for 45 minutes before analyzed by LC-MS. The chromatograms shown represent UV-Vis absorbance. The identity of product **5** was confirmed by matching to standard with MS/MS spectrum. The identity of product **7** was confirmed indirectly by comparing its MS/MS and UV-Vis spectra with those of related compounds.

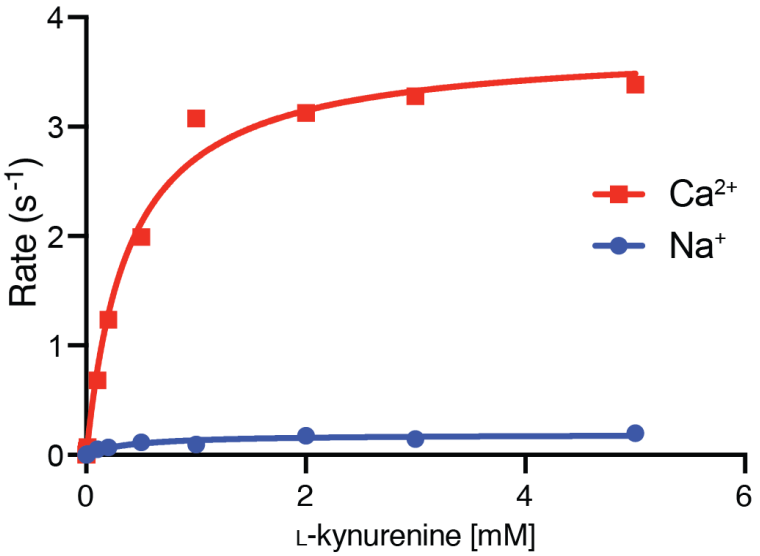

Figure S7 | Kinetic analysis for *Pc*ncAAAD against L-kynurenine. Assays were conducted in a 50 mM Tris pH 8.0 reaction buffer containing either 30 mM Na^{+} or Ca^{2+}. Production of **4** was measured by LC-MS and compared against a standard curve of the authentic standard. Data collected were fitted with Michaelis–Menten nonlinear regression model.

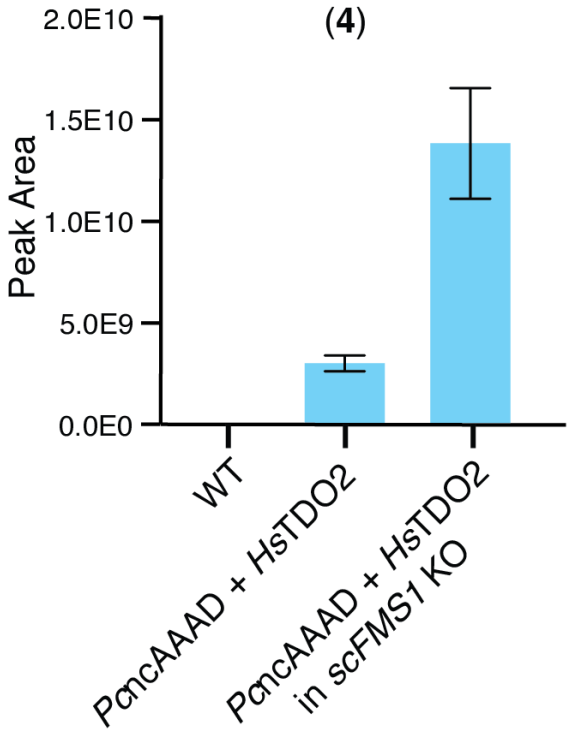

Figure S8 | Expression of *HsTDO2* and *PcncAAAD* in the *scFMS1* knockout (KO) strain resulted in the accumulation of 4. Bar graph indicates the integrated peak area of **4**. The production of **4** increased in *scFMS1* KO strain suggests the role of *sc*FMS1 in the oxidation of biological monoamines. Error bars represent SEM of biological triplicates.

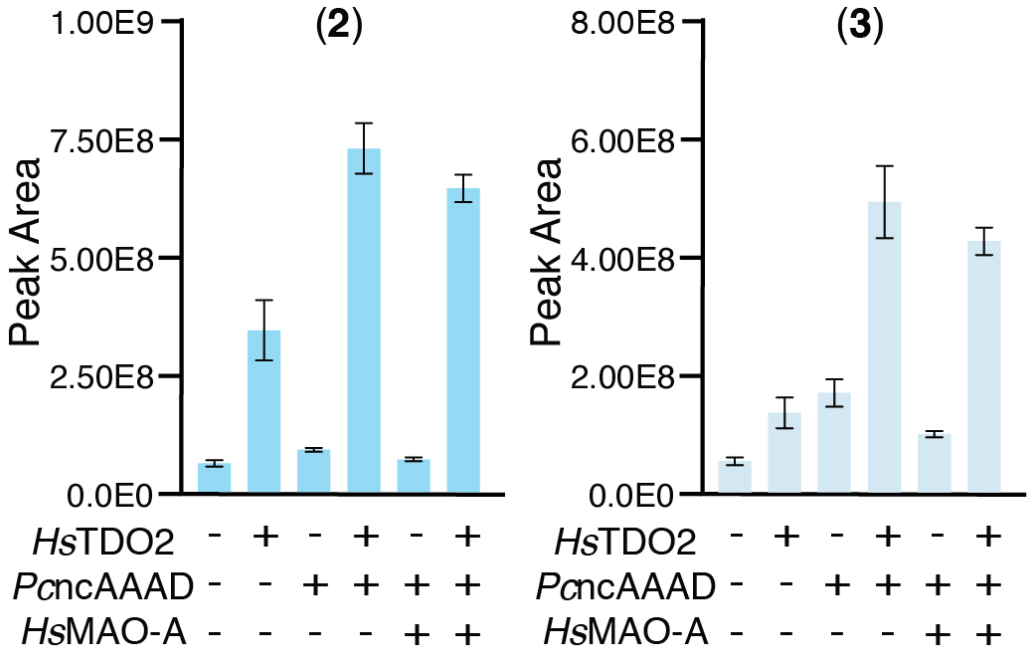

Figure S9 | Production of 2 and 3 in various engineered yeast strains. Production of **2** and **3** significantly increased in the engineered three-gene pathway. Error bars represent SEM of biological triplicates.

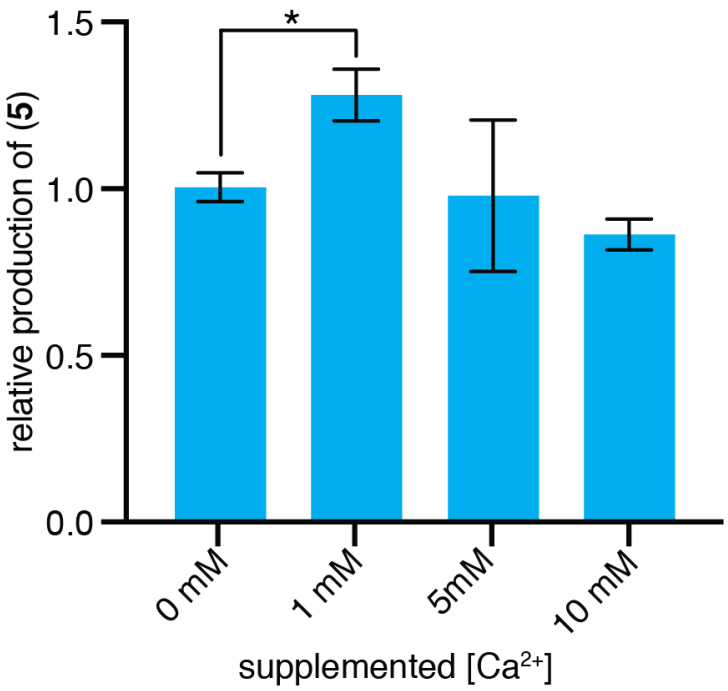

Figure S10 | Calcium-dependent production of 5 in engineered yeast. The bar graph shows the relative production of **5** in yeast, when the media was supplemented with 0, 1, 5, or 10 mM calcium chloride. The production peaks at 1 mM supplemented Ca^{2+}, with a 1.3-fold increase compared to 0 mM supplemented Ca^{2+}. The increase in the product accumulation is likely due to calcium-dependent acceleration of *Pc*ncAAAD activity while the decrease is likely caused by the toxicity of high concentration calcium. Note that the growth medium YNB contains ~0.9 mM calcium ion. Error bars represent SEM of biological triplicates. The asterisk indicates that the *p*-value is less than 0.05.

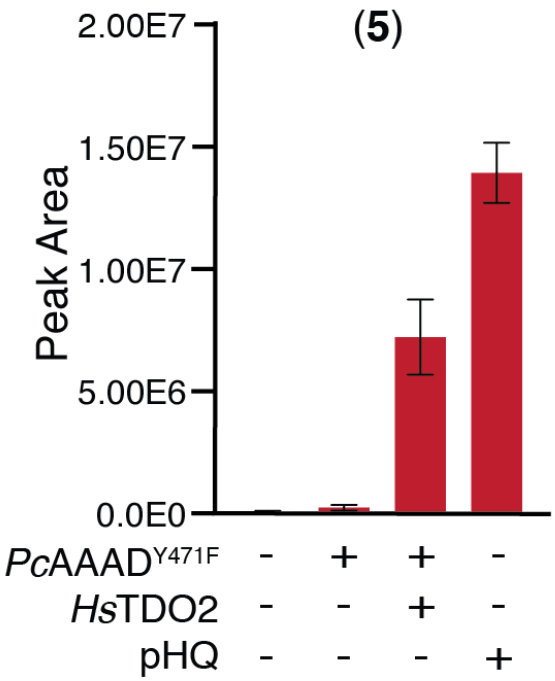

Figure S11 | The relative production of 5 across various engineered yeast strains. The *Pc*ncAAAD ^{Y471F} mutant is expected to function as an aldehyde synthase capable of converting L-kynurenine to **5** in a single enzymatic step; however, *Hs*TDO2 and *Pc*ncAAAD ^{Y471F} coexpression strain produces less **5** than the pHQ strain.

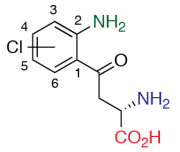

chloro-L-kynurenine
5-Cl: **9a**
4-Cl: **9b**
3-Cl: **9c**

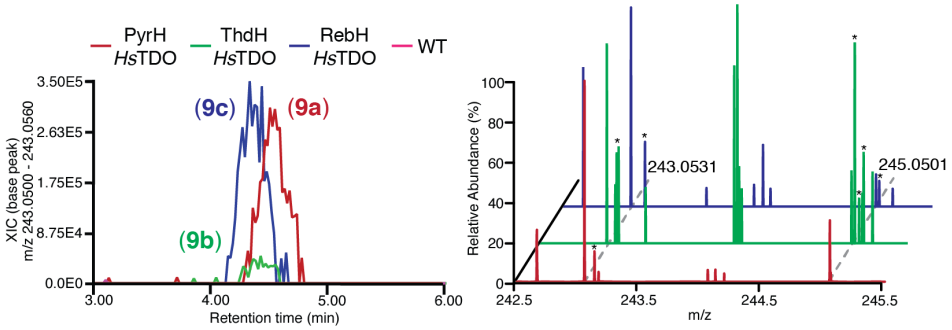

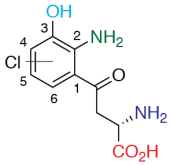

chloro-3-hydroxy-L-kynurenine
5-Cl: **10a**
4-Cl: **10b**

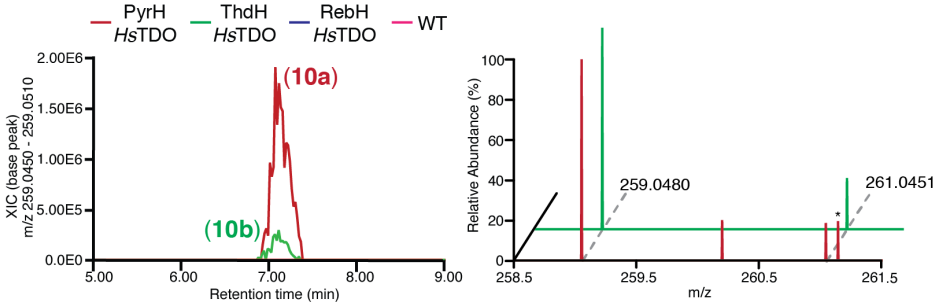

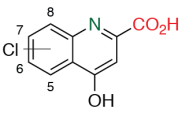

chloro-2-carboxy-4-hydroxyquinoline
6-Cl: **11a**
7-Cl: **11b**
8-Cl: **11c**

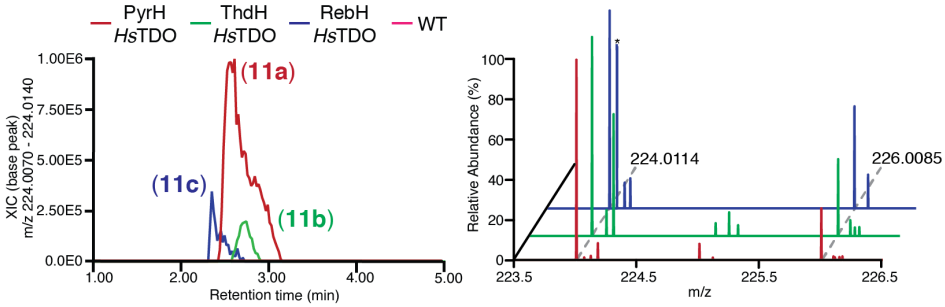

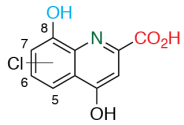

chloro-2-carboxy-4,8-dihydroxyquinoline
6-Cl: **12a**
7-Cl: **12b**
8-Cl: **12c**

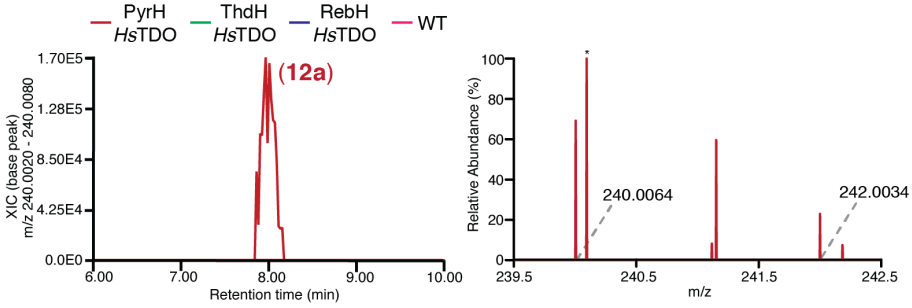

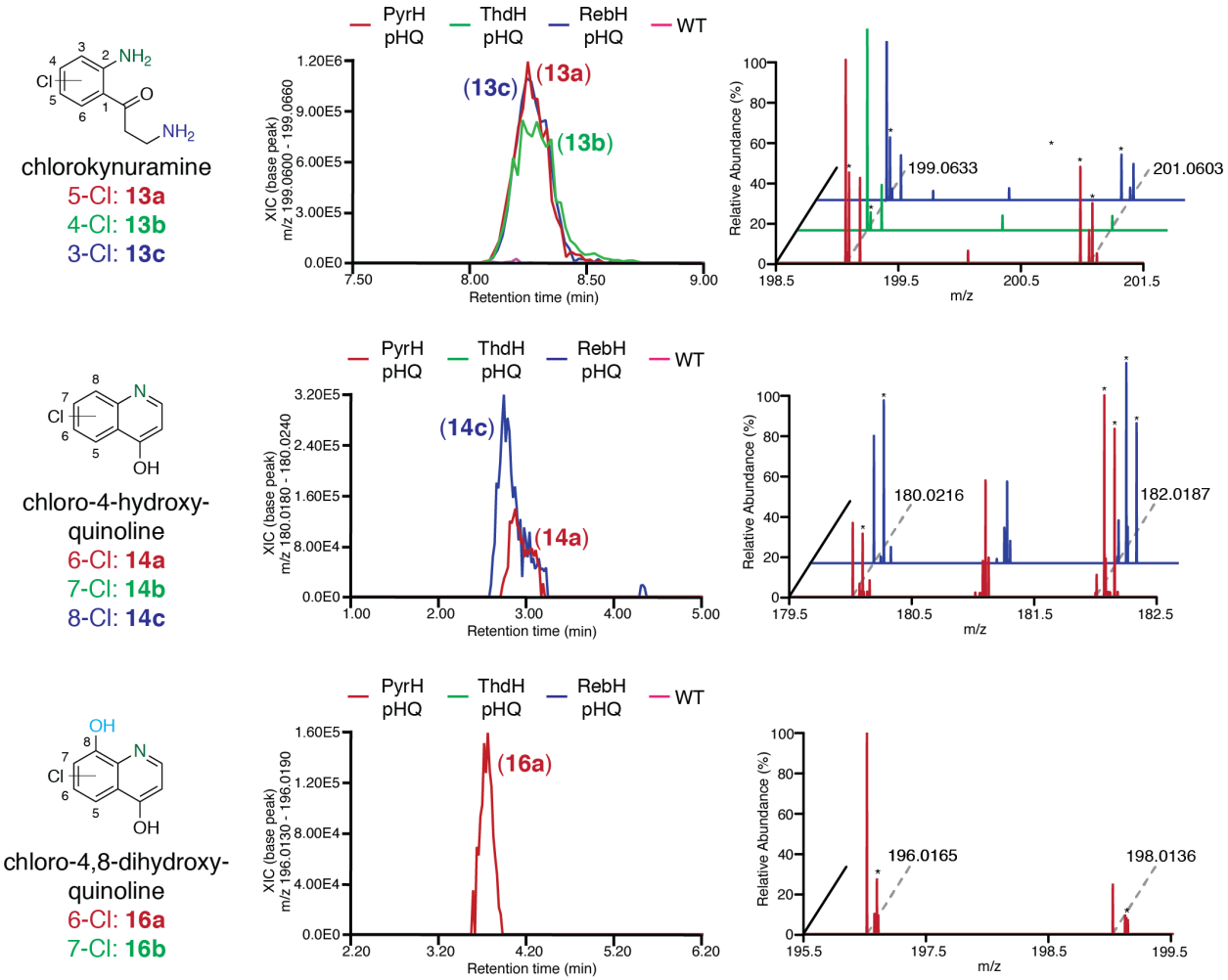

Figure S12 | LC-MS chromatograms and isotope patterns of chlorinated molecules produced from engineered yeast. Chlorinated molecules (left), their LCMS chromatograms (middle), and the isotope patterns observed at the corresponding peak (right) are shown. In the isotope pattern panel, the masses of Cl^{35}- and Cl^{37}-incorporated molecule are shown. Impurity peaks are noted with asterisks. Isotope patterns are not in a perfect 3:1 ratio, which could reflect the kinetic isotope effect of some enzymatic reactions.

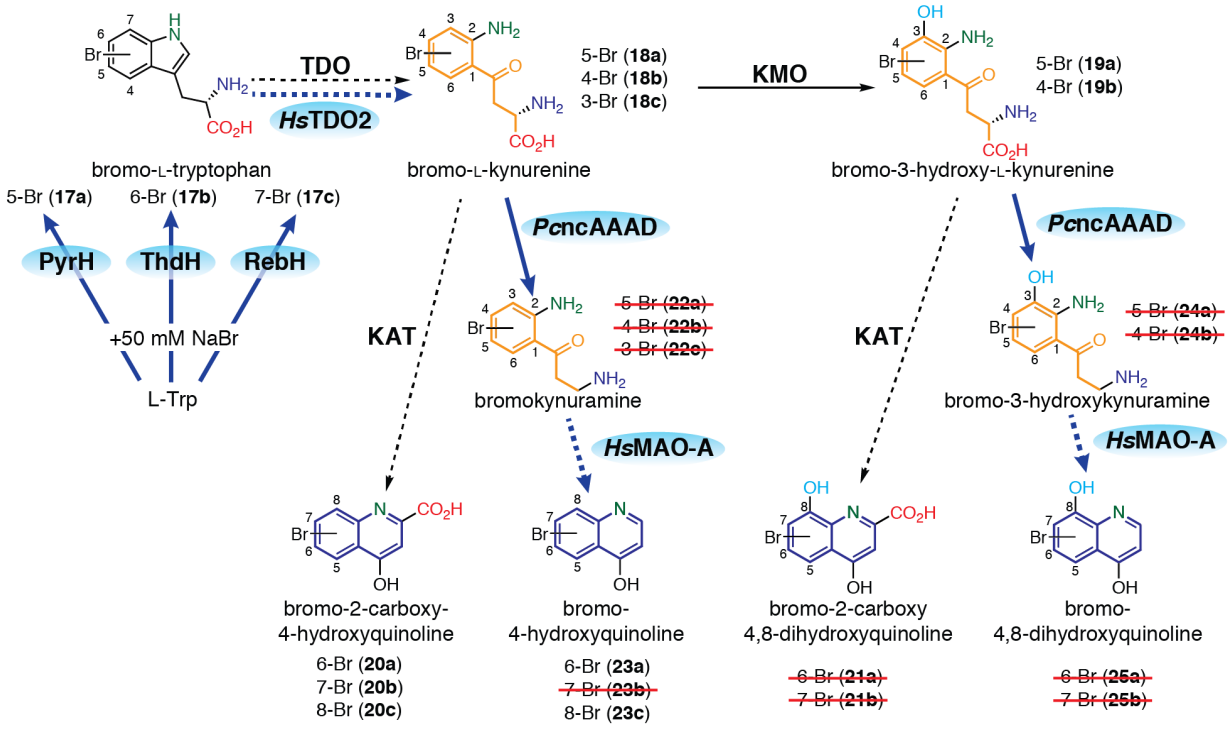

Figure S13 | Engineered pathway to produce brominated kynurenine-pathway-derived molecules. The ability of the halogenases PyrH, ThdH, and RebH to incorporate bromine onto L-tryptophan is exploited to further derivatize the kynurenine-derived products. Similar to the expanded kynurenine pathway displayed in **Figure 1**, compounds **17-20** and **23**, analogs of L-tryptophan, L-kynurenine, **1**, **2**, **4**, and **5** with bromination at different positions on the aromatic ring were produced. The LC-MS chromatograms and isotope patterns of these molecules are shown in **Figure S14**. Compounds crossed with a red line are ones that were not observed, which could be due to either the instability of the molecules or the inability of the engineered pathway to accommodate certain halogenated intermediates.

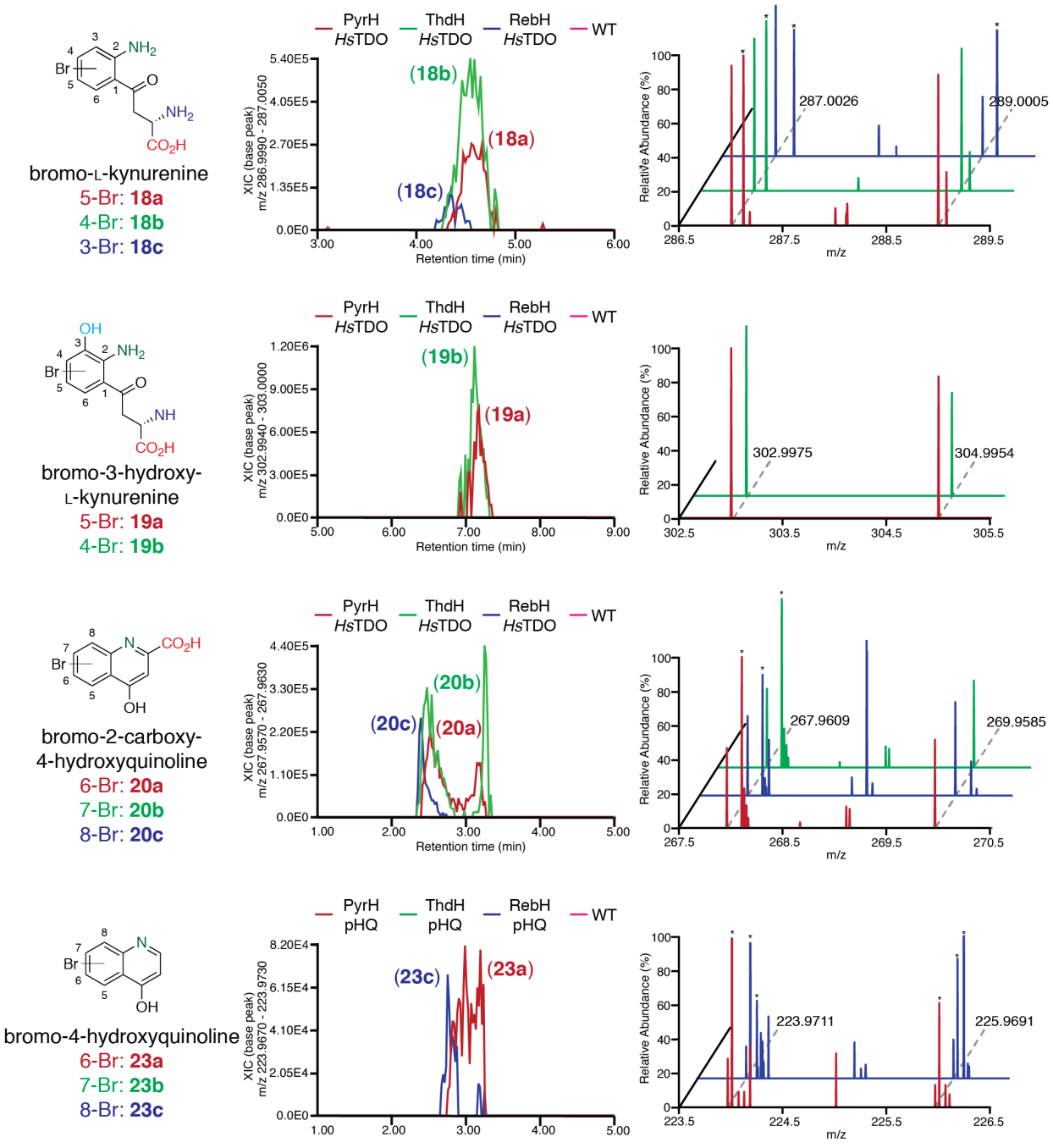

Figure S14 | LC-MS chromatograms and isotope patterns of brominated molecules produced from engineered yeast. Brominated molecules (left), their LCMS chromatograms (middle), and the isotope patterns observed at the corresponding peak (right) are shown. In the isotope pattern panel, the masses of Br^{79}- and Br^{81}-incorporated molecule are shown. Impurity peaks are noted with asterisks. Isotope patterns are not in a perfect 1:1 ratio, which could reflect the kinetic isotope effect of some enzymatic reactions.

TABLES

Table S1. Cloning primers.

Gene	Vector/ purpose	Direction	Sequence
*Pc*ncAAD	pHis8-4	F	GAAAACTTGTACTTCCAGGCCCATGGCATGCCTTCCAGTCACCCTCACATTACTC
*Pc*ncAAD	pHis8-4	R	CTCGAATTCGGATCCGCCATGGCTACTTCGTCGGAGCAACAGTCTCCAATTTG
*Pc*ncAAD	p423TEF	F	GCATAGCAATCTAATCTAAGTTTTCTAGAACTAGTATGCCTTCCAGTCACCCTCAC
*Pc*ncAAD	p423TEF	R	CAGCCCGGGGGATCCACTAGTCTACTTGGCGGGAGCGATAGTCTC
*Pc*ncAAD	pYTK001	F	GCATCGTCTCATCGGTCTCATATGCCTTCCAGTCACCCTCACATTACTC
*Pc*ncAAD	pYTK001	R	ATGCCGTCTCAGGTCTCAGGATCTACTTCGTCGGAGCAACAGTCTCCAATTTG
*Pc*ncAAD	Mutation	F	GCTTGGACGAGGAAACGCCAGTATATC
*Pc*ncAAD	Mutation	R	GATATACTGGCGTTTCCTCGTCCAAGC
*Pc*ncAAD	Mutation	F	CGAAGTAAAGAGGCGCATGGGAC
*Pc*ncAAD	Mutation	R	GTCCCATGCGCCTCTTTACTTCG
HsTDO2	p425TEF	F	ATAGCAATCTAATCTAAGTTTTCTAGAACTAGT ATGAGTGGGTGCCCATTTTTAGGAAAC
HsTDO2	p425TEF	R	CAGCCCGGGGGATCCACTAGT TTAATCTGATTCATCACTGCTGAAGTAGGAGC
HsTDO2	pYTK001	F	GCATCGTCTCATCGGTCTCATATGAGTGGGTGCCCATTTTTAGGAAAC
HsTDO2	pYTK001	R	ATGCCGTCTCAGGTCTCAGGATTTAATCTGATTCATCACTGCTGAAGTAGGAGC
HsTDO2	Mutation	F	GCAGTTTTCCATTCTGGAAACGATGACAGCCTTGG

HsTDO2	Mutation	R	CCAAGGCTGTCATCGTTTCCAGAATGGAAAACTGC
HsMAO-A	p426TEF	F	AGCAATCTAATCTAAGTTTTCTAGAACTAGT ATGGAGAACCAAGAAAAGGCTTCTATCGC
HsMAO-A	p426TEF	R	CAGCCCGGGGGATCCACTAGTTCAGGATCTAGGCAAAAGTTTATAC TTATATAATAC
HsMAO-A	pYTK001	F	GCATCGTCTCATCGGTCTCAT ATGGAGAACCAAGAAAAGGCTTCTATCGC
HsMAO-A	pYTK001	R	ATGCCGTCTCAGGTCTCAGGAT TCAGGATCTAGGCAAAAGTTTATACTTATATAATAC
RebH	pYTK001	F	GCATCGTCTCATCGGTCTCATATGTCAGGAAAGATCGACAAAATAC TAATTGTGGG
RebH	pYTK001	R	ATGCCGTCTCAGGTCTCAGGATCTATCTTCCGTGTTGTTGACGTAA GAATTCATGTAAG
RebF	pYTK001	F	GCATCGTCTCATCGGTCTCATATGACAATCGAGTTTGACCGTCCAG G
RebF	pYTK001	R	ATGCCGTCTCAGGTCTCAGGATCTAGCCCTCTGGGGTCCAGAC
PyrH	pYTK001	F	GCATCGTCTCATCGGTCTCATATGATCCGTAGTGTTGTAATCGTCG GG
PyrH	pYTK001	R	ATGCCGTCTCAGGTCTCAGGATCTATTGGATGCTTGCAAGGTACTC GTAACA